KARMA

Karst **A**quifer **R**esources availability and quality in the **M**editerranean **A**rea

Application of lumped parameter modelling at the KARMA test sites

Deliverable 4.2

Authors: Guillaume Cinkus (UM), Naomi Mazzilli (AU), Hervé Jourde (UM), Christelle Batiot-Guilhe (UM), Andreas Wunsch (KIT), Tanja Liesch (KIT), Zhao Chen (KIT), Marco Petitta (URO), Valeria Lorenzi (URO), Chiara Sbarbati (URO), Juan Antonio Barberá Fornell (UMA), Bartolomé Andreo Navarro (UMA), Nataša Ravbar (KRI), Joanna Doummar (AUB), Rachida Bouhlila (ENIT), Emna Gargouri Ellouz (ENIT), Fairouz Slama (ENIT), Nico Goldscheider (KIT)

Date: September 2021

This project has received funding from the European Union's PRIMA research and innovation programme

Technical References

Project Acronym	**KARMA**
EU Programme, Call and Topic	PRIMA, Multi-topic 2018, Water resources availability and quality within catchments and aquifers
Project Title	Karst Aquifer Resources availability and quality in the Mediterranean Area
Project Coordinator	Prof. Dr. Nico Goldscheider, Karlsruhe Institute of Technology (KIT), nico.goldscheider@kit.edu
Project Duration	September 2019 - August 2022
Deliverable No., Name	D4.2 Application of lumped parameter modelling at the KARMA test sites
Dissemination Level*	Public (PU)
Work Package	WP4: Modelling Tools
Task	Task 4.2: Development of lumped-parameter and artificial neural network models
Lead beneficiary	Karlsruhe Institute of Technology (KIT)
Contributing beneficiary/ies	Bundesanstalt für Geowissenschaften und Rohstoffe (BGR), University of Malaga (UMA), University of Montpellier (UM), Sapienza University of Rome (URO), Ecole nationale d'Ingenieurs de Tunis (ENIT), American University of Beirut (AUB)
Due Date	Month 18
Actual Submission Date	

* PU = public

CO = Confidential, only for members of the consortium (including the Commission Services)

RE = Restricted to a group specified by the consortium (including the Commission Services)

Version History

Version	Date
1.0	September 2021

Project Partners

(Coordinator)

Participant No *	Organisation	Country
1 **(Coordinator)**	Karlsruhe Institute of Technology (KIT)	Germany
2 **Partner 1**	Federal Institute for Geosciences and Natural Resources (BGR)	Germany
3 **Partner 2**	University of Malaga (UMA)	Spain
4 **Partner 3**	University of Montpellier (UM)	France
5 **Partner 4**	University of Rome (URO)	Italy
6 **Partner 5**	American University of Beirut (AUB)	Lebanon
7 **Partner 6**	Ecole National d'Ingénieurs de Tunis (ENIT)	Tunisia
8 **External expert** **	Karst Research Institute (KRI)	Slovenia

** N. Ravbar contributed to this deliverable in her role as external expert / member of the project advisory board

Executive Summary

KARMA (Karst Aquifer Resources availability and quality in the Mediterranean Area) is a European project that aims to achieve substantial progress with respect to the hydrogeological understanding and sustainable management of Mediterranean karst water resources at various temporal and spatial scales.

WP4 proposes new approaches to the characterization and hydrodynamic modelling of karst systems, based on conceptual models, neural networks, and physical models. The aim is to build lumped-parameter and ANN models to simulate karst spring discharge on the KARMA test sites, and subsequently (i) to identify and understand the principal processes that dominate the overall behaviour of these karst systems, (ii) to improve predictions concerning impacts of extreme events, such as floods and droughts, and (iii) to help forecasting flash-floods at short timescale. This document addresses Task 4.2 (Development of lumped-parameter and ANN models).

For this task, KARMA data from all sites were used in spite of a delayed start for some partners due to the COVID-19. Additionally, three other sites have been included in the KARMA project for this modelling work: (i) Gottesacker karst system, which is located at the border between Germany and Austria and has been monitored hourly for 10 years - data from the office of the federal state of Vorarlberg, division of water management. Oberstdorf station data is from German Meteorological Service. (ii) Unica karst system, which is a large Slovenian karst system - data from the Slovenian Environment Agency has been considered at a daily timestep for the period 1961-2018 (ARSO, 2021), and (iii) Gato Cave system, which is a Spanish karst system monitored at a daily timestep since 1963.

Table of Content

1 Introduction

Around 9% of the world's population is dependent on karst water resources for drinking water (Stevanović, 2019). Understanding the functioning of these complex and heterogeneous systems is therefore a major challenge for water resource management. Among many tools used is karst hydrology, modelling is a key approach that helps to characterize the hydrological functioning of karst systems and identify the principal processes that dominate their overall behaviour. Numerous modelling approaches such as lumped, artificial neural network (ANN), and physical-based are used to support the sustainable water resource management of karst aquifers (Jeannin et al., 2021).

Discharge modelling has been widely used in hydrology to gain insight into the functioning of hydrosystems. The analysis of karst hydrological response through models is a powerful way of developing knowledge of the internal processes. It can be used to look into the hydrological functioning and structure of a system and identify the main processes and factors at stake. At catchment scale, modelling can be used also to assess groundwater recharge and to estimate the dimensions of the catchment.

This work aims to evaluate the characteristics of several Mediterranean karst systems through lumped-parameter modelling, to better quantify groundwater recharge and karst storage from precipitation and floodwater. Another objective is to make the link between the previous Task on the typology of karst systems (4.1) and the structure of the models, to provide guidelines for helping in the design of models and limit the choice of parameters.

This report is divided into five main sections:

- Section 2 introduces the lumped parameter modelling approach
- Section 3 presents the karst systems analyzed in the study
- Section 4 shows the dataset used for each site
- Section 5 presents the results of the snow module for 5 KARMA test sites
- Section 6 provides preliminary analyses on the precipitation-discharge relationship
- Section 7 presents the model structures, the modelling approach and the results

2 Lumped parameter modelling

The purpose of the lumped-parameter modelling approach is to gain insights into the functioning of a karst system, in order to better respond to the problems of water management and preservation.

2.1 Principle

Lumped-parameter (or reservoir) models are a conceptual representation of a hydrosystem, which involves the association of several reservoirs that are thought to be representative of the main processes at stake. They are connected to each other through flow equations that turn an input signal (precipitation and evapotranspiration) into an output signal (discharge at spring). Each reservoir is described by a variable, its water height, and several parameters related to the flow equation that translates the water height into a discharge (either linear or puissance laws). The parameters are defined through calibration against observed data.

A lot of lumped-parameter models have been developed to study the relation between precipitation and discharge in karst systems (Hartmann et al., 2014). They all differ in complexity regarding the number of reservoirs and parameters, which have to be well-thought in order to preserve physical realism and limit equifinality on model parameters. Careful sensitivity analyses and uncertainty assessment should be considered along with the results of the models to avoid over interpretations (Refsgaard et al., 2007).

Lumped-parameter models can be seen as a trade-off between simulation performance and insight into the functioning of a system. This approach is well suited to karst systems as there is a high heterogeneity and usually little knowledge of system structure (Fleury et al., 2009; Hartmann et al., 2012).

2.2 The KarstMod platform

2.2.1 Description

KarstMod is an adjustable modelling platform that provides a modular, user-friendly interface for simulating spring discharge at karst outlets and analysing the hydrodynamic functioning of the different compartments considered in the model (Mazzilli et al., 2019). The general structure of the KarstMod model is based on the following conceptual model of a karst aquifer (Mazzilli et al., 2019):

- **The infiltration zone** (soil and epikarst) drains water from the surface through a vertical network of fissures and conduits. Storage of water may occur in the unsaturated zone, as well as local saturation;
- **The saturated zone** comprises a dual porosity functioning, with a network of high permeability fractures and conduits, and a low permeability matrix with a high storage capacity.

The model structure can go up to four reservoirs (Figure 1) with one on the upper level that translates the processes occurring in the soil and epikarst zone, and three on the lower level that may be connected with the former and correspond to the infiltration and/or saturated zones. The discharge can be simulated with (i) several linear and non-linear water level – discharge laws, (ii) a hysteretic water level – discharge function for reproducing the hysteretic functioning observed on the wet-dry cycles in the unsaturated zone (Lehmann et al., 1998; Tritz et al., 2011), and (iii) an exchange function that aims to reproduce the interactions between matrix and conduits.

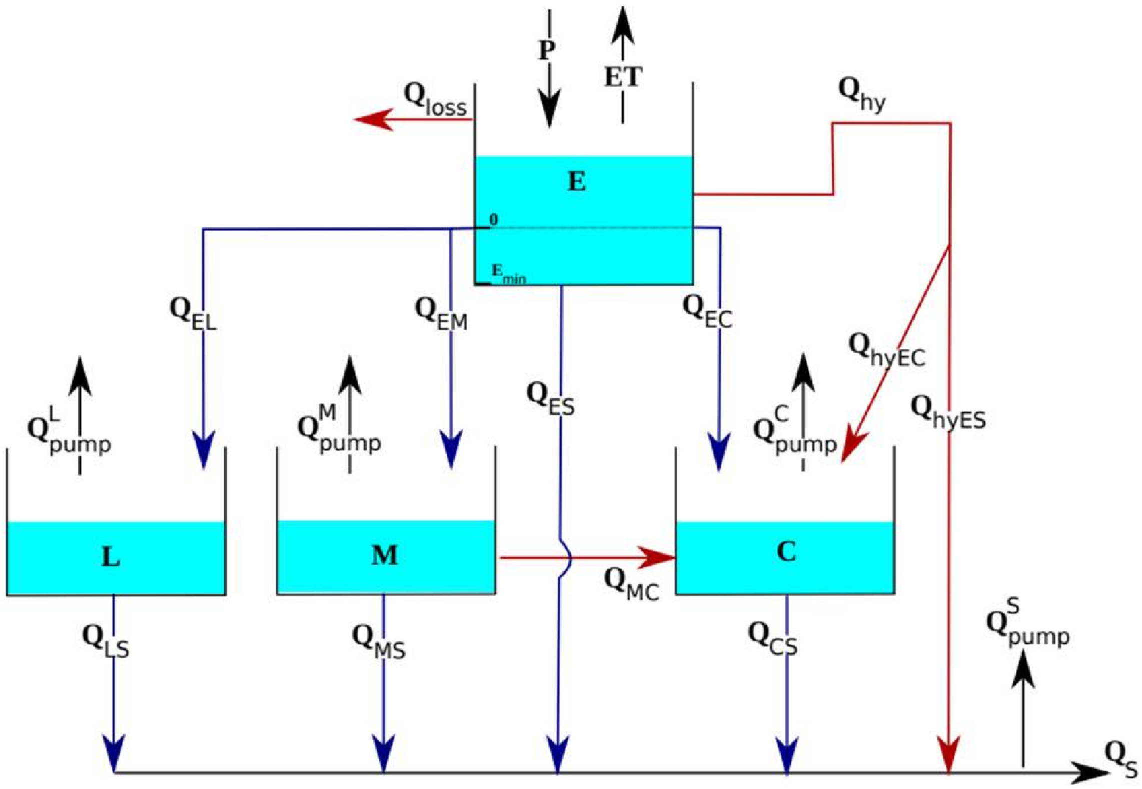

Figure 1: Structuration of the KarstMod platform (Mazzilli et al., 2019).

More details about the balance equations, the parameters involved and the KarstMod platform in general can be found in (Mazzilli et al., 2019) or in the KarstMod User Guide (Mazzilli and Bertin, 2019).

2.2.2 Input data and workflow

The model requires rainfall, evapotranspiration and observed discharge time series over the period of concern. Pumped discharge time series can be provided and associated to a specific compartment (L, M, C) or to the discharge before the outlet (S). Piezometric level time series can be used for calibration and validation. A basic spline interpolation can be realised on the discharge dataset to fill eventual gaps in the time series.

The user has to define the performance measure (detailed in next section 2.2.3) and the periods of warm-up, calibration and validation. The warm-up period needs to be long enough for the model to adjust and reach an optimal state. The calibration period is the period over which the parameters offer the best results according to the performance measure. The validation period is to evaluate the relevance of the parameters on a time interval that is not used for calibration purpose.

2.2.3 Performance criteria

Four performance criteria are proposed in the KarstMod model to evaluate the results of the simulation:

- The Nash-Sutcliffe Efficiency coefficient NSE (Nash and Sutcliffe, 1970), which is based on the sum of the squared errors. This criterion tends to favour the high discharges due to the quadratic nature of the equation;

$$NSE = 1 - \frac{\sum(Q_s - Q_{obs})^2}{\sum(Q_{obs} - \overline{Q_{obs}})^2}$$

- The Volumetric Efficiency VE (Hogue et al., 2006), which is the measure of the bias between simulated and observed discharges;

$$VE = 1 - \frac{\sum |Q_s - Q_{obs}|}{\sum Q_{obs}}$$

- The modified Balance Error BE (Perrin et al., 2001), which involves to compare the simulated and observed discharge regarding the mass balance of the considered period. It is usually associated with another criterion;

$$BE = 1 - \left|\frac{\sum Q_s - \sum Q_{obs}}{\sum Q_{obs}}\right|$$

- The Kling Gupta Efficiency KGE (Gupta et al., 2009), which is based on the NSE and aims to limit some of its bias in a more balanced way.

$$KGE = 1 - \sqrt{(r-1)^2 + (\alpha - 1)^2 + (\beta - 1)^2}$$

With Q_s and Q_{obs} the simulated and observed discharges (or the equivalent piezometric level), r is the Pearson correlation coefficient between the simulated and observed discharge, β is the ratio between the mean simulated and mean observed discharge and α is the ratio between the simulated and observed flow variance. Applied to discharge modelling, the three components help to evaluate distinct errors between simulated and observed discharges: (i) r is related to shape and timing (Santos et al., 2018); (ii) β focuses on the difference in discharged volumes; and (iii) α looks at the flow variability.

The criteria can range from $-\infty$ to 1. A performance criterion of 1 for NSE, VE or KGE means a perfect match between simulated and observed discharge, while for BE it means that the volume of water at the total volume discharged at the outlet is equal for simulated and observed time series.

KarstMod platform allows to associate until 2 of these criteria, with a ponderation factor as well as the possibility to apply the criteria above or below user-defined threshold.

2.3 Snow routine: implementation to KarstMod as an external module

The account of snow accumulation and melt in hydrological modelling can greatly enhance the results of the models, especially for regions where the snow volume is significant. Chen et al. (2018) successfully simulated spring discharge of a mountainous karst system heavily influenced by snow accumulation and melt. They applied a modified version of the HBV snow routine Bergström (1992) proposed by Hock (1999). We used this snow routine as an external KarstMod module (i.e. without intern calibration), but we consider to further implement the module into the KarstMod platform for directly calibrating the parameters of the snow routine.

This snow routine simulates snow accumulation and melt over different sub-catchments defined based on altitude ranges. The input data consist in three time series (temperature, precipitation and potential clear-sky solar radiation) and five parameters (temperature threshold, melt coefficient, refreezing coefficient, radiation coefficient and water holding capacity of snow). The potential clear sky solar radiation time series and radiation coefficient are only used when working at an hourly time scale to simulate a more refined snowmelt by considering sun exposure. We manually calibrated temperature threshold, melt coefficient and radiation coefficient.

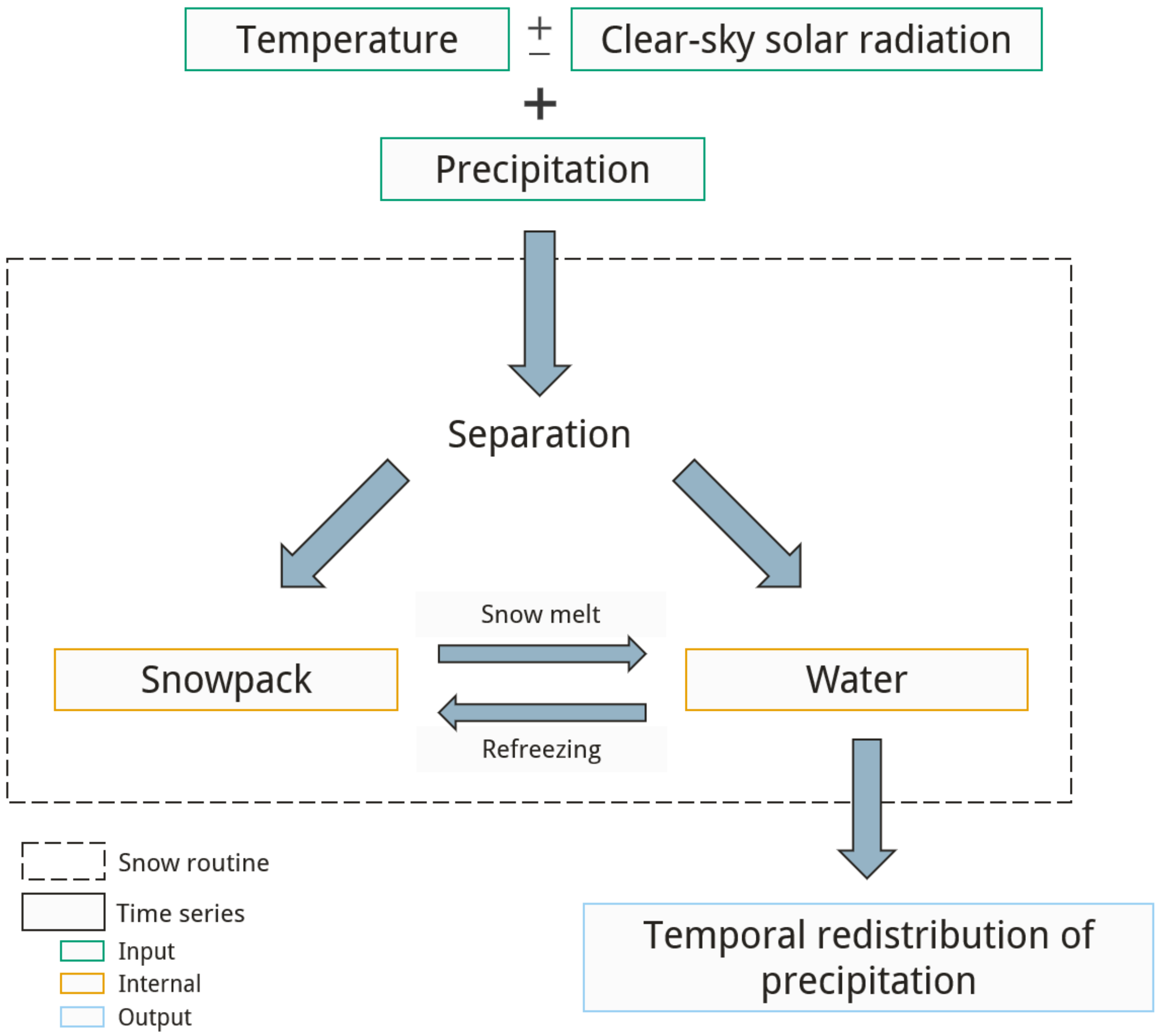

Figure 2: Snow routine workflow.

The workflow is presented in Figure 2. The precipitation is considered as snow when the air temperature is lower than the temperature threshold. Snowmelt starts with the temperature above the threshold according to a degree-day expression, where snowmelt is function of the melt coefficient, the solar radiation and the degrees above the threshold. Runoff starts when the liquid water holding capacity of snow is exceeded. The refreezing coefficient is for refreezing liquid water in the snow if snow melt is interrupted (Bergström, 1992). The output of the snow routine is a redistributed precipitation time series.

3 Description of the test sites

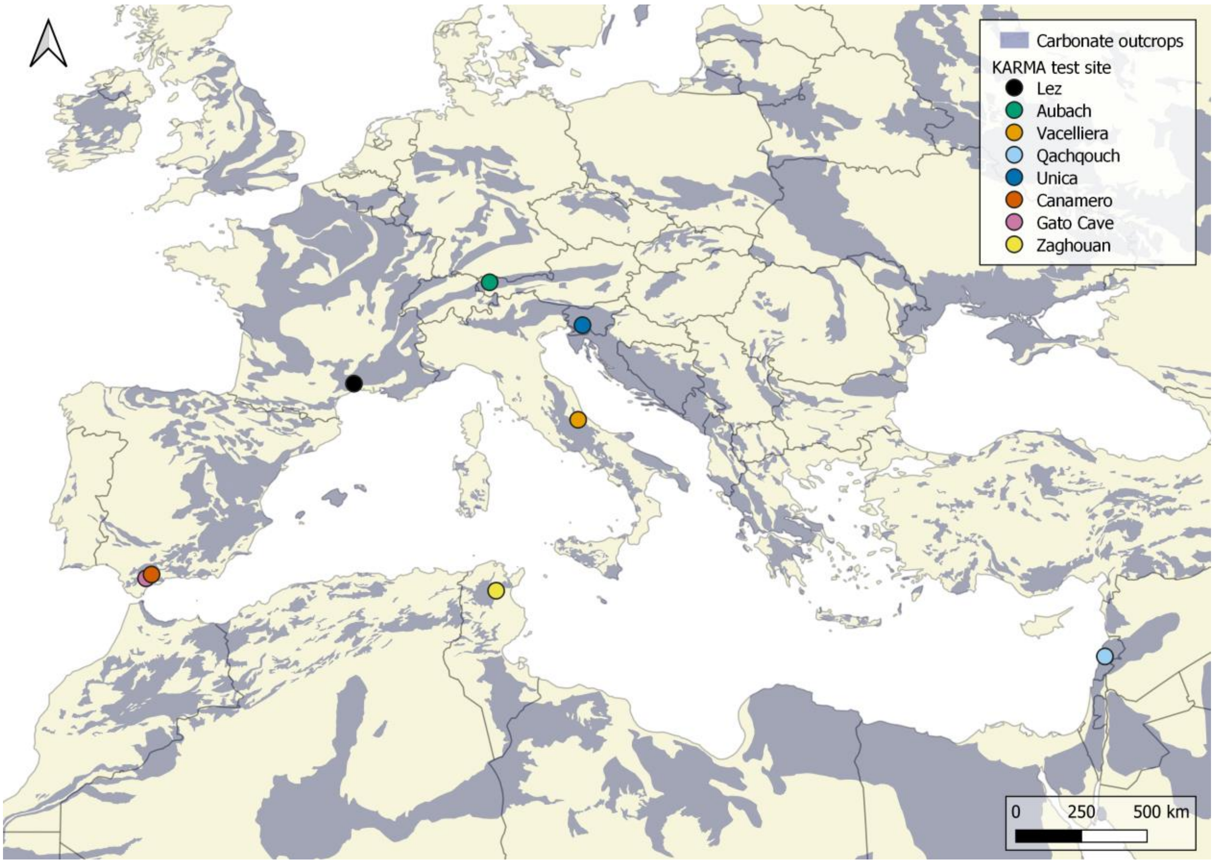

Figure 3: Localisation of the KARMA test sites (delimitation of carbonate outcrops after Chen et al. (2017)).

The Table 1 and Figure 3 display an overview of the main characteristics of the KARMA test sites (Figure 3).

Table 1: Summary of the main characteristics of the KARMA test sites.

Country	Spring	Köppen-Geiger climate classification	Catchment area	Mean discharge	Mean annual precipitation
			km^2	$m^3.s^{-1}$	mm
France	Lez*	Csa	130	0.91	904
Germany/Austria	Aubach	Dfc	9	0.91	2089
Italy	Vacelliera	Dfb/Dfc	1.3	0.06	1491
Lebanon	Qachqouch	Csa	56	2.01	1258
Slovenia	Unica	Dfb	>820	21.97	1505
Spain	Canamero	Csa	NA	0.92	900
Spain	Gato Cave	Csa	NA	1.50	1852
Tunisia	Zaghouan	Csa/BSk	19	0.10	500

*Discharge under anthropogenic forcing. The mean total discharge including water abstraction is about 2 $m^3.s^{-1}$.

Five of the test sites are located on the Mediterranean area (Lez, Qachqouch, Canamero, Gato Cave and Zaghouan) with a temperate climate, dry and hot summer (Csa) according to Köppen-Geiger classification (Peel et al., 2007). The three other sites (Aubach, Vacelliera and Unica) are located in mountainous regions in inland areas with continental climate and no dry season. Aubach system is classified with cold summer (Dfc), Unica is classified with warm summer (Dfb) whereas Vacelliera is classified as a mix of Dfb and Dfc.

3.1 France

The Lez spring catchment is located 15 km north of Montpellier (France). It is located between the Hérault and Virdoule river valleys. The maximum extent of the hydrogeological basin which feeds the Lez spring is estimated to be about 380 km^2, on the basis of the area affected by regional drawdown resulting from continuous pumping at the karst spring (Thiéry and Bérard, 1983). The lithology of the Lez karst system corresponds to massive limestone of the Upper Jurassic (Argovian to Kimmeridgian) and of the lower part of the Early Cretaceous (Berriasian), with 650 to 1000 m thickness (Avias, 1995). The marls and marly-limestone of the Middle Jurassic (Oxfordian) constitute the lower boundary of the aquifer. The marls and marly-limestone of the Early Cretaceous (respectively Lower and Upper Valanginian) constitute the upper boundary of the aquifer (Mazzilli, 2011). The major tectonic events that influenced the Lez aquifer were: the Hercynian/Variscan orogeny, the Pyrenees formation, and the opening of the Lion Golf (Avias, 1995).

As a large part of the hydrogeological catchment is relatively impermeable, due to the presence of marls and marly-limestones of the Valanginian, the effective Lez spring recharge area covers about 130 km^2 only (Fleury et al., 2009), which corresponds to the Jurassic limestone outcrops located at the western and northern limits of the basin. Localized infiltration occurs through fractures and sinkholes along the basin and through the major geologic fault of Corconne-Les Matelles, in the northern part of the basin. A certain number of fractures are also known to appear only just upstream from the Lez spring. The Lez catchment is exposed to a Mediterranean climate, which is characterized by hot, dry summers, mild winters and wet autumns. Analyses by the Meteo France show that on average 40% of the annual precipitation occurs between September and November with a high variability across years (Bicalho et al., 2012). The average annual rainfall rate for the 1945-2019 period is 916 mm based on a weighted average of four rainfall stations located on the Lez basin.

The Lez system is under anthropogenic pressure (i.e. aquifer exploitation for water supply) with pumping performed directly within the karst conduit. The discharge is measured at the spring pool and is regularly null during low water periods, when the pumping rate exceeds the natural spring discharge.

3.2 Germany

Aubach spring is located within the Hochifen-Gottesacker area at the border between Germany and Austria (northern Alps). The system is part of a bigger catchment of about 35 km^2 with an altitude that varies between 1000 m and 2230 m above sea level (Chen et al., 2018), which is highly concerned with snow accumulation and melt. The Gottesacker catchment can be divided into karst and non-karst areas, with highly karstified Schrattenkalk limestone formations on the northern part and impermeable sedimentary rocks of the Flysch zone in the southern part, which connect through the Schwarzwasser valley (Goldscheider, 2005). The Aubach spring is thus influenced by several temporary springs that occur upstream and by inflow from the Flysch area where the surface runoff may sink into an estavelle and connect via an underground connection during low flow periods.

The meteorological data come from three stations that are located outside of the catchment at a lower altitude. The mean annual precipitation is 1836 mm with snow accumulation occurring generally between November and May (Chen et al., 2018). The estimation is slightly lower than the one of the current dataset due to the consideration of a different time period (2012-2020 for our study).

3.3 Italy

The Gran Sasso hydrostructure is a calcareous-karstic aquifer system containing one basal regional aquifer of more than 700 km^2 of total extension of carbonate outcrops. The main springs have been organized into six groups based on groundwater flow and hydrochemical characteristics, as illustrated in (Figure 4). The aquifer has a total discharge of more than 18 m^3/s from its springs (Amoruso et al., 2013), including a highway tunnel drainage tapped for drinking water on both sides.

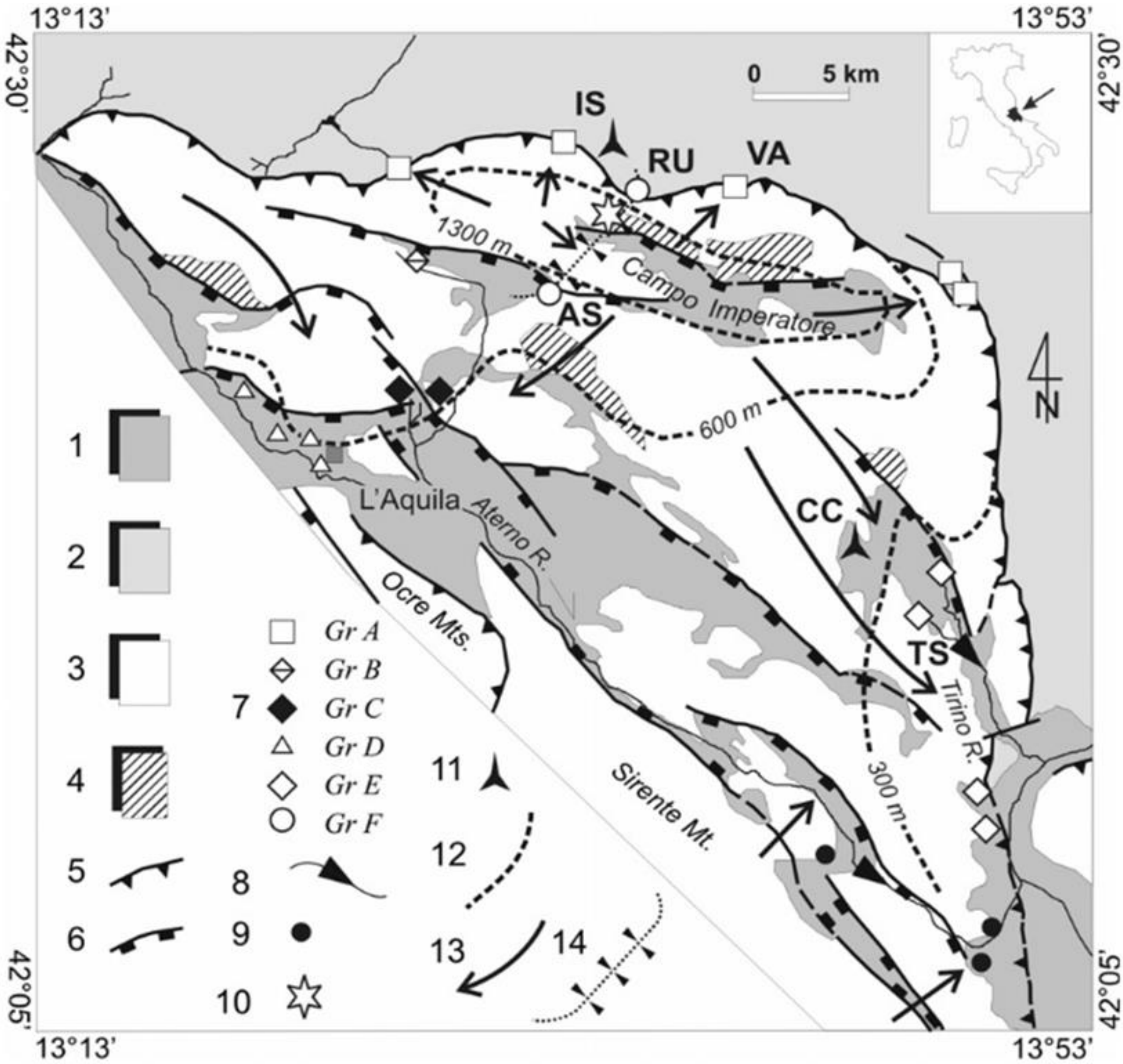

Figure 4: Gran Sasso hydrogeological outline. 1: aquitard (continental detrital units of intramontane basins, Quaternary); 2: aquiclude (terrigenous turbidites, Mio-Pliocene); 3: aquifer (calcareous sequences of platform Meso-Cenozoic); 4: low permeability substratum (dolomite, upper Triassic); 5: thrust; 6: extensional fault; 7: main spring: AS: Assergi drainage; RU: Ruzzo drainage; VA: Vacelliera spring: TS: Tirino springs; symbols refer to the six spring groups identified in Barbieri et al. (2005); 8: linear spring; 9: springs belonging to a nearby aquifer; 10: INFN underground laboratories; 11:

meteorological station (IS: Isola Gran Sasso, CC: Carapelle Calvisio); 12: presumed water table in m asl; 13: main groundwater flow path; 14: highway tunnels drainage (after Amoruso et al., 2013).

The spring taken into account for the application of lumped parameter modelling, is the Vacelliera Alta spring, being part of the Vacelliera spring group. The entire group is located on the northern side of the Gran Sasso aquifer. It is considered as representative of the overflow of the aquifer along the no-flow regional thrust of the Gran Sasso. The Vacelliera spring is fed by shallow water flow that overlaps the groundwater coming from the regional baseflow. The latter comes out at the tectonic contact between the Meso-Cenozoic limestone complex and the Miocene terrigenous complex (Petaccia and Rusi, 2008). The mean discharge of the total Vacelliera spring group, completely tapped by the Ruzzo aqueduct for drinking water purposes, is about 0.168 m^3/s, with a significant variability with seasons and years.

The Vacelliera Alta spring is located about 1018 m a.s.l. and it is fed by a hydrogeological basin of about 1.30 km^2 with an average discharge of 0.053 m^3/s measured in the period between 2000 and 2020 (Figure 5). The catchment area has been defined basing on geological setting and annual water balance. Moreover, its altitude varies between 1200 m and 2300 m above sea level. Hydrographs of the Vacelliera Alta spring shows a gradual increase due to seasonal recharge in the wintertime, typical of Apennine springs fed by the regional aquifer. Seasonal recharge is in fact mainly due to snowmelt that plays a significant role on aquifer recharge and consequently of spring feeding. The catchment area is affected mainly by snowfall during winter and fall time (Jan- Apr and Nov-Dic). The climatic station of Campo Imperatore has been considered to define meteoric events such as snow and rain. It is located in the central region of the ridge at 2152 m a.s.l.. The obtained recharge of the catchment area of Vacelliera Alta spring is influenced by the rainfall (1110 mm/y) and by the melting of the snowpack (the data has been converted from cm of snow to mm of rainfall of about 265.66 mm/y) for a total average recharge over a long period (2000-2020) of about 1376 mm/y.

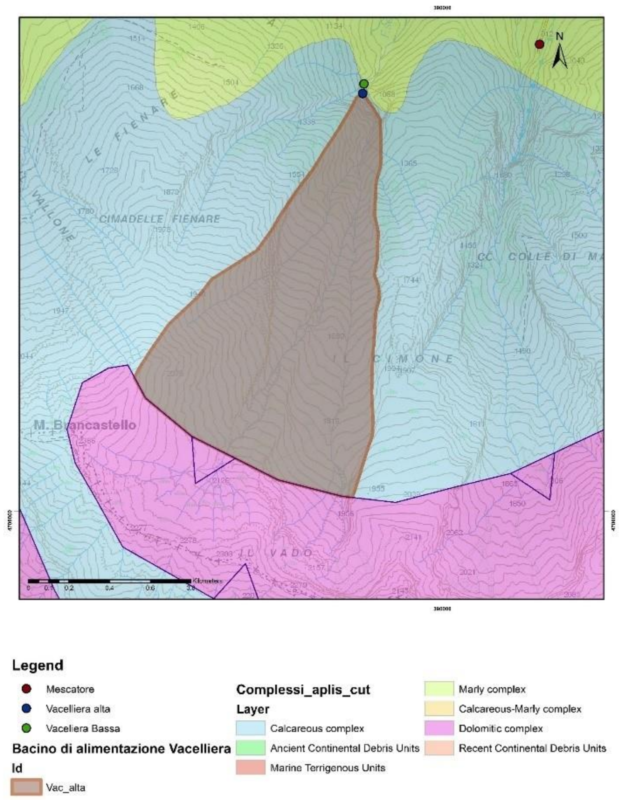

Figure 5: Position and catchment area (with brown border) of the Vacelliera Alta spring and the related hydrogeological complexes.

3.4 Lebanon

Qachqouch spring is located within the Nahr el-Kalb catchment and originates from the Jurassic karst aquifer at about 64 m above sea level. The recharge area is estimated of approximately 56 km^2 with an elevation ranging between 60 to more than 1500 meters above sea level (Dubois et al., 2020). During low flow periods, the spring is used to complement the water deficit in the capital city Beirut and surrounding areas. The total yearly precipitation is estimated from two stations to about 950-1500 mm on average, with a limited snow accumulation.

The lithology of the surface water and groundwater catchments mostly consists of Jurassic karstified limestone and dolomitic limestone (in the higher plateaus) grading into more massive micritic limestone in the lower portion of the catchment. Formations of middle cretaceous age are exposed on the upper parts of the catchment. The Qachqouch system is characterized by a duality of flow in a low permeability matrix and high permeability conduit system (Dubois, 2017). The elongated shape of the catchment may influence the hydrological response depending on the location of the precipitation.

3.5 Slovenia

The catchment of the Unica springs, which recharge a typical karst polje, is a complex binary karst system with a recharge area estimated to be about 820 km^2. It is subdivided into three subcatchments (Gabrovšek et al., 2010), with prevailing (i) allogenic infiltration from two subcatchments drained by sinking rivers that cross a chain of karst poljes and a river valley, and (ii) autogenic infiltration through a karst plateau with highly karstified limestone (Gabrovšek et al., 2010; Kovačič, 2010; Petric, 2010). The poljes follow each other in a downward series and are connected in a common hydrological system. Being characterized by a surface river network and frequent flooding, this induces a very particular response at the Unica springs with very high hydrological variability (by many orders of magnitude), as well as delayed and prolonged high-flow values (Mayaud et al., 2019). In the past 60 years, there has been a slight increase in forest cover but a sudden large-scale forest disturbance (ice breakage, bark beetle infestation, windthrow) occurred in the period 2014-2018. This significant change in land cover induced increases in effective precipitation (less canopy infiltration and evapotranspiration) and observed discharge of the Unica River (Kovačič et al., 2020).

Unica river is fed by two springs and several temporary springs. The mean joint discharges is 21 m3.s-1 in the period 1989-2018 with average annual precipitation estimated at 1505 mm for Cerknica station (Kovačič et al., 2020). Unica spring discharge exhibit slow and rapid flow components as well as matrix-conduits exchanges. The low water periods are sustained by flows from the karstified limestone area, which has a significant groundwater storage (Gabrovšek et al., 2010). The soil over the catchment is between 0 and 30 cm on the karstified limestone but thicker on the dolomites and flyschs of the allogenic subcatchments. A part of the discharge is lost due to underground bifurcation (Kogovšek et al., 1999).

3.6 Spain

3.6.1 Canamero

Canamero spring is part of the Sierras of Merinos-Colorado-Carrasco karst systems. Jurassic limestones cover a large area in the test site and these lithologies are represented on surface, as karst exposures, or in depth, as buried aquifer segments. Dolomitic rocks, which comprise the lower levels of the Jurassic aquifers, can reach higher positions in the lithological sequence, and even appear on surface. Gypsum bearing formations (Triassic clays with gypsum), whose thickness is still imprecise, constitute the lower limit of the main aquifers and can uplift through faults. The drainage of the aquifer occur through multiple springs and a groundwater transference toward the porous aquifer of the Ronda basin. The mean annual precipitation is about 733 mm (Barberá, 2014).

3.6.2 Gato Cave

Gato Cave spring is part of the Sierra de Lìbar karst system, which has an area of 103 km^2 and two other major outlets (Andreo et al., 2006). The site is mainly represented by Jurassic dolomites and limestones, and Cretaceous marls and marly limestones (Algarra, 1987). There are well-developed karst features such as karrenfields, vertical shafts and cave systems. Several poljes are present in the synclines on the Cretaceous marls outcrops, which generate surface flow during rainfall. Soil is absent on limestone and dolomite outcrops, and present on marls outcrops. The mean annual precipitation is over 1500 mm (Andreo et al., 2006).

3.7 Tunisia

The Zaghouan massif extends from the East-west extension valley of the Rmal wadi in the north, to the transversal syncline of Loukanda. The Zaghouan anticline is mainly constituted by Jurassic limestone and is characterized by the presence of southern and transverse faults that have created individualized blocks. The region of Zaghouan is characterized by an upper semi-arid to subhumid climate with an average annual rainfall of 467 mm presenting heterogeneous spatial distribution and a large time fluctuation (from 245 mm to 625 mm).

Djebel Zaghouan aquifer is one of the most important water resources of good quality in the region and is currently exploited for water supply via several boreholes.

4 Input data

The data used for modelling is presented in Table 2. We worked with observed discharge (Q), precipitation (P) and evapotranspiration (either AET when available or PET) time series on each site at the more refined time-step available, which is daily for Lez, Vacelliera, Qachqouch, Unica, Canamero, Gato Cave and Zaghouan, and hourly for Aubach. The length of the observations varies from 2 to 58 years. The Lez dataset is provided with an actual evapotranspiration time series, as well as a pumped discharge and piezometry time series that were considered in the modelling process.

We handled missing values in the different time series as follows: (i) temperature gaps have been interpolated linearly, (ii) precipitation and ET gaps have been considered equal to 0, and (iii) discharge gaps have been interpolated with a Lagrange polynomial function. Maximum observed gaps are detailed in Table 2. Note that on Lez system, we observed maximum gaps of 17 and 16 days for pumped discharge and piezometric level, respectively.

Table 2: Details on meteorological and hydrological input data and characteristics of the time series.

Country	System	Data considered	Timestep	Length of the observations (year)	Maximum gap (days)			
					P	T	Q	ET
France	Lez	Q, P, AET, Qpump, Z	Daily	10 (2008-2018)	0	2	7	0
Germany/Austria	Aubach	Q, P, PET	Hourly	8 (2012-2020)	0	0	0	0
Italy	Vacelliera	Q, P, PET	Daily	3 (2017-2020)	3	4	6	0
Lebanon	Qachqouch	Q, P, PET	Daily	5 (2015-2020)	0	0	11	0
Slovenia	Unica	Q, P, PET	Daily	58 (1961-2018)	0	1	0	29
Spain	Canamero	Q, P, PET	Daily	3 (2007-2010)	0	0	34	0
Spain	Gato Cave	Q, P, PET	Daily	52 (1963-2015)	0	0	0	0
Tunisia	Zaghouan	Q, P, PET	Daily	2 (1915-1917)	0	/	0	0

5 Estimation of the snow component

The snow routine was applied on systems with either occasional snow episodes (Lez, Qachqouch) or significant snow coverage (Aubach, Vacelliera, Unica). It was not possible to apply the snow routine on Zaghouan system due to the lack of temperature data, although the snow influence of the hydrological functioning is thought to be significant. The snow accumulation was considered negligible on the Gato Cave and Canamero catchment.

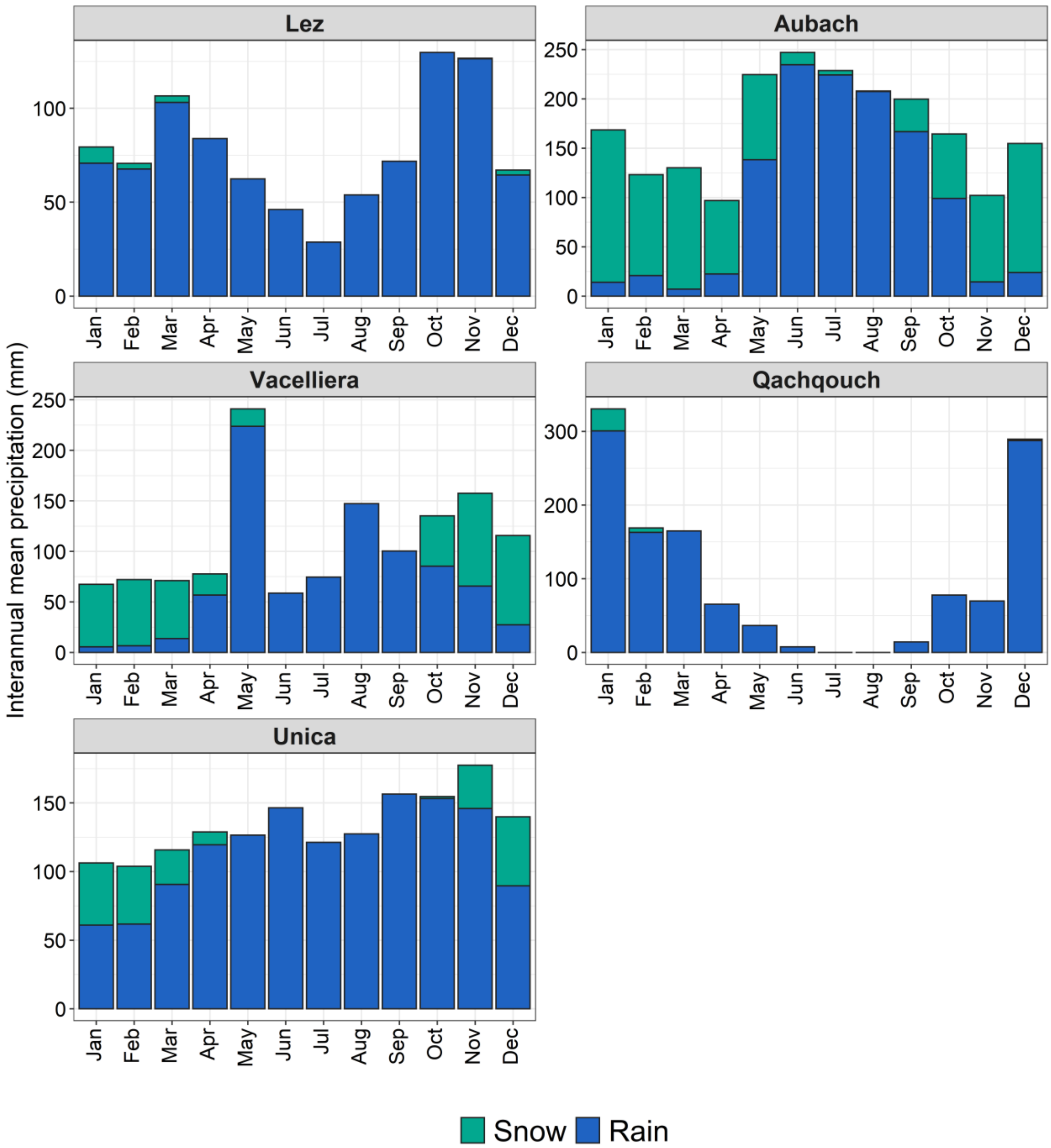

Figure 6: Distribution of snow accumulation and rain calculated within the snow module.

Snow accumulation represent about 1.9%, 42.6%, 33.8%, 3.2%, and 12.8% of the total precipitation on the studied period for the Lez, Aubach, Vacelliera, Qachqouch and Unica systems, respectively (Figure 6). Snow occurs in the winter months (November to April) on all sites. Significant snowfall events were recorded at Lez, Aubach, Vacelliera, Qachqouch and Unica sites with a maximum 3 consecutive day snow accumulation of 40 mm, 125.7 mm, 74.3 mm, 30.5 mm and 126.1 mm, respectively.

6 Systemic analysis of rainfall-discharge relationship

6.1 Results of the classification

Classification is a first-line tool for understanding the main characteristics of a natural system's response. We evaluated the functioning of the systems over the periods of concern according to the classification initially proposed in Deliverable 4.1, which has been revised in Cinkus et al. (2021, submitted). The classification is based on recession curves analysis and consists in 6 different classes. Karst systems functioning are differentiated with three indicators through their capacity of dynamic storage (k_{max}), the draining dynamic of their capacitive function (α_{mean}) and the variability of their hydrological response (IR). We performed (i) correlational and spectral analyses to evaluate the regulation time (RT), which gives insight into the global inertia of a system; and (ii) analysis of classified discharges, to assess the presence or absence of major specific functioning.

Six of eight systems (Lez, Aubach, Qachqouch, Unica, Canamero and Gato Cave) have a low dynamic storage and a fast draining of the capacitive function, which indicates a large degree of karstification.

Lez (Appendix 1) and Aubach (Appendix 2) are classified C2 with a very fast draining of the capacitive function, which correspond to a highly reactive functioning. In the case of the Lez system, the indicator is probably biased by the continuous pumping into the saturated zone of the aquifer. According to Mangin's interpretation grid of classified discharges (Mangin, 1971), the absence of bending points on the curve indicates a homogeneous functioning regardless of the hydrological conditions. This result is not consistent with the current knowledge of the overflow Lirou spring. For Aubach, there are no evident bending points on the curve of classified discharges. However, the continuous curvature could be related to the activation of overflow outlets, to flows outside the system, or a temporary storage of water (which are detailed in Chen and Goldscheider (2014)).

Qachqouch (Appendix 4) and Unica (Appendix 5) are classified C3 with a high variability of the hydrological functioning, which indicates a relation between the hydrological response and the saturation state of the system. For Qachqouch, the dampened response in wet periods may be due to the elongated shape of the catchment, which contributes to the filtration and the slow restitution of the precipitation at the spring. The small bending point at 5 m^3/s^{-1} could be related to the activation of an overflow outlet, to flows outside the system, or a temporary storage of water. For Unica, the dampened response may be due to the extraordinary size and complexity of the system with autogenic and allogenic recharge. The continuous draining and flooding of the multiple poljes maintain high water levels in the aquifer system. The values above the bending point on the curve of classified discharges at 85.5 m^3/s^{-1} refer to rather sporadic and exceptional flood events (Ravbar et al., 2021). Then the polje fed by the springs is completely flooded and the conditions consequently present accurate measurements of the flow values.

Canamero (Appendix 6) and Gato Cave (Appendix 7) are classified C4 with a low variability of the hydrological response. The springs' responses are quite steady, regardless of the saturation state of the system. For Canamero, the bending point at 3.5 m^3/s^{-1} may be due to the activation of an overflow outlet, a discharge to another system, or a temporary storage of water, but it is not excluded that it can be related to uncertainties on ungauged discharges. For Gato Cave, there are no bending points on the curve of classified discharges, which indicates that there is no major specific functioning on the system.

Vacelliera (Appendix 3) and Zaghouan (Appendix 8) are classified C6 with a very high capacity of dynamic storage, a very slow draining of the capacitive function, and a very low variability of the hydrological response. These characteristics are typical of little or no karstified systems with a high capacity to filter the precipitation signal and a consistent hydrological functioning. For Vacelliera and Zaghouan, the respective bending points at 0.06 m^3/s^{-1} and 0.09 m^3/s^{-1} could be related to the activation of an overflow outlet, to flows outside the system, or a temporary storage of water.

6.2 Statistical analysis of precipitation and discharge

We first performed a qualitative description of monthly mean interannual discharge against monthly mean interannual redistributed precipitation (Figure 7). The shape of the redistributed precipitation time series fits well with the shape of changes in discharge, especially for Aubach, Vacelliera and Unica where the snow influence is significant. Their hydrological regimes are characterized by floods occurring in the spring due to snow melt and in autumn due to precipitation. The hydrological regimes of Lez, Qachqouch, Canamero and Gato Cave systems are characterized by floods in winter and spring, and low flow periods in summer. The dry period is much more pronounced on the Qachqouch system (June-November) than the two others. The shift between discharge and precipitation on Zaghouan system (January/April) may be explained by the non-consideration of the snow influence on the catchment.

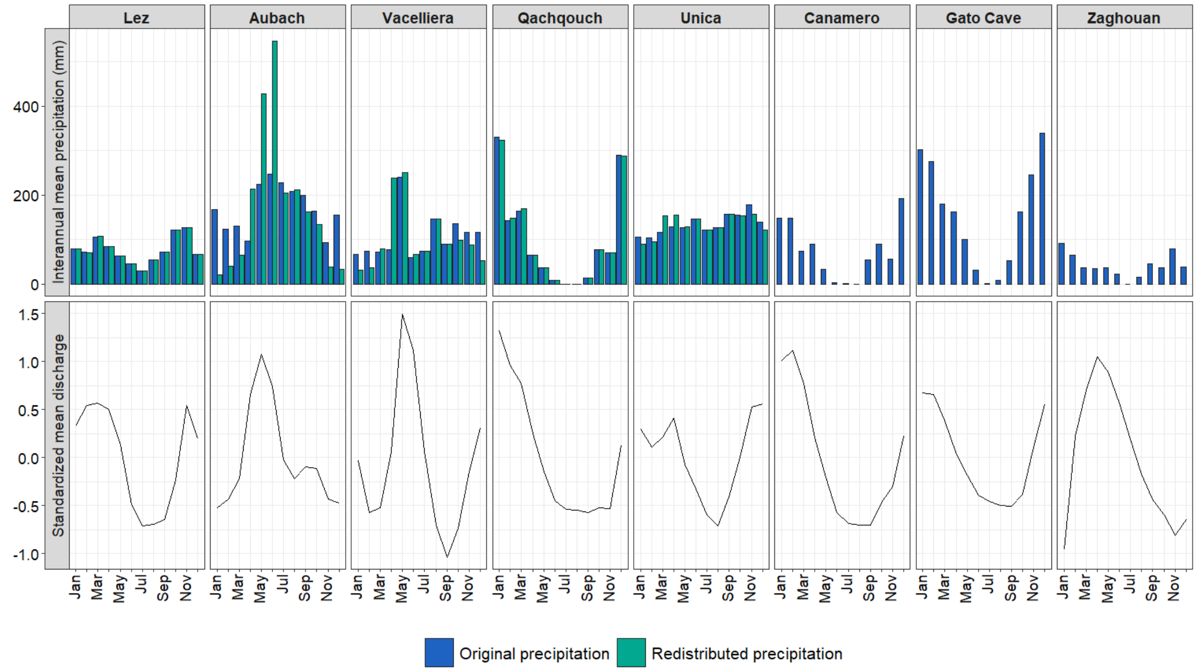

Figure 7: Interannual monthly statistical analyses of precipitation and discharge.

Second, we performed cross correlational analyses between (redistributed) precipitation and discharge on each site (Figure 8). Cross correlational analyses are time series analyses that are used to study the relation between two signals. The principle is to examine the transformation of the input signal into an output signal (Padilla and Pulido-Bosch, 1995). The maximum value of the cross-correlation coefficient gives insight into the system capacity of filtration of the precipitation signal. The decrease of the cross-correlation coefficient with time is related to the emptying of the aquifer. The response time, which corresponds to the time lag for the maximum value of the cross-correlation coefficient, is related to the dynamics of the functioning of the system.

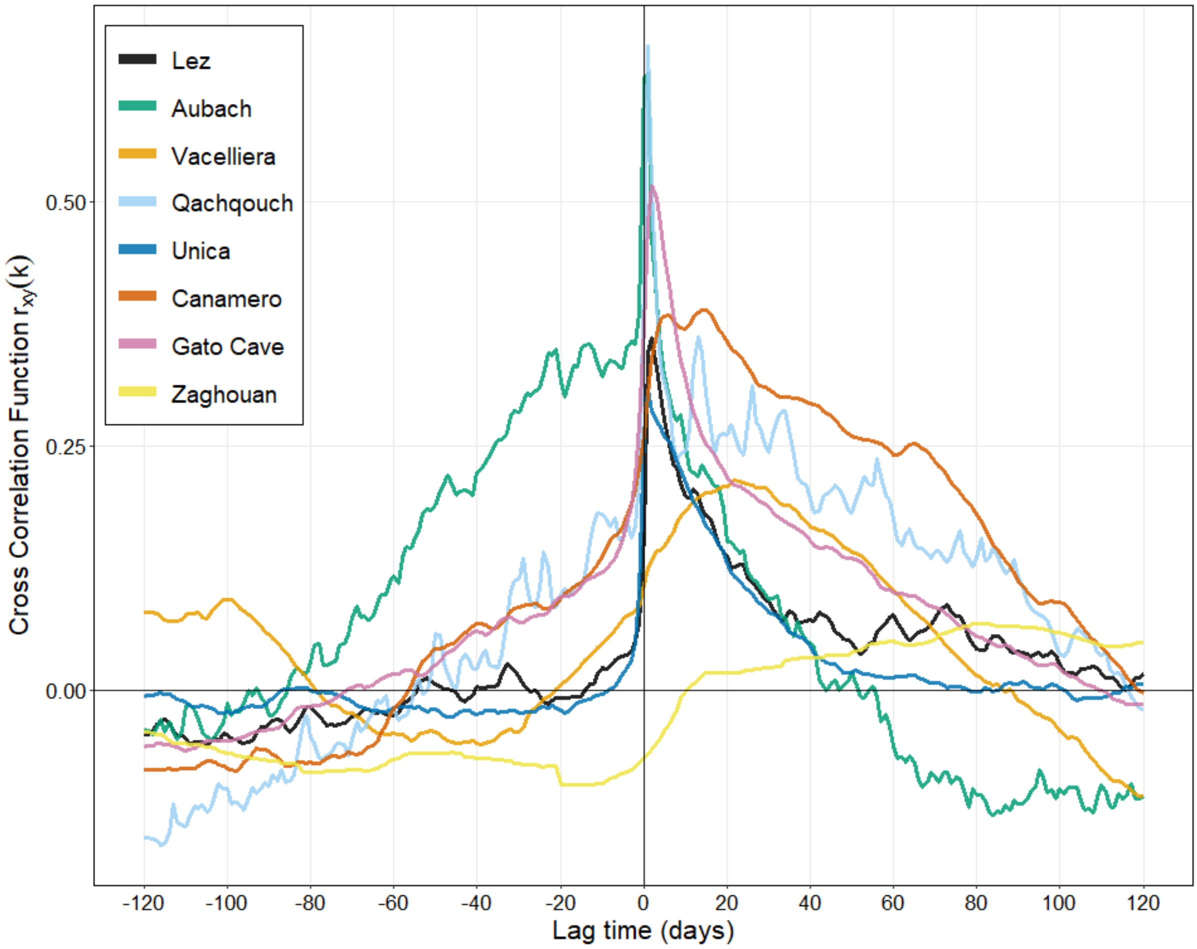

Figure 8: Cross correlation analyses of precipitation and discharge.

The cross-correlation functions of Lez, Aubach, Qachqouch, Unica and Gato Cave are characterized by a sharp peak followed by a quick decrease during 10 to 20 days. It indicates a good transmissivity of the water into conduits, likely associated with an efficient connectivity. The low response times (about to 1 day for Aubach, Qachqouch, Unica, and 2 days for Lez and Gato Cave) highlight a fast transfer of the quick component through the system, especially for Aubach, Qachqouch and Unica, which may have an hourly response time that cannot be caught at daily timescale (n.b. we performed the analysis at a daily time scale on Aubach spring for the comparison with the other test sites). The high peak values of the cross-correlation function for Aubach, Qachqouch and Gato Cave (0.63, 0.66 and 0.52, respectively) indicate a very low filtration of the precipitation signal in the first few days. The cross-correlation functions of Lez, Qachqouch, Unica and Gato Cave are also characterized by slower decrease from 30, 20, 40, and 20 days respectively. It may translate a slow filtration of a part of the precipitation in the capacitive function of these systems, especially for Qachqouch and Gato Cave. For the Lez system, this slow decrease may be biased by the consecutive null values during summer when the spring dries out. The cross-correlation function of Qachqouch is characterized by several peaks every 5-10 days, which can be either related to the elongated shape of the catchment or due to noise in the signals.

The signals of Vacelliera, Canamero and Zaghouan do not exhibit a quick decrease in the first days after a precipitation input, but only a slow decrease through all the hydrological response. It can be explained by a much less karstified, even close to mainly fractured, system for Vacelliera and Zaghouan systems. The response time of Canamero is between 4 and 12 days and may indicate a good capacity of filtration of the precipitation signal in the system. The response times of Vacelliera and Zaghouan are greater than 20 days and the correlation coefficients are rather low compared to the other sites, which confirm the inertial functioning of those systems. Similarly, as the statistical analyses of precipitation and discharge (section 6.2), the non-consideration of the snow influence on Zaghouan catchment likely induces a bias in the cross-correlational analysis.

The results of the cross-correlation analyses are mainly consistent with those of the classification (section 6.1), except for Lez and Gato Cave. Aubach (C2) is highly reactive with a fast draining of the system. Lez (C2) is reactive but does not exhibit a fast draining, which may be due to the continuous pumping into the saturated zone that influences the result of the classification. Qachqouch and Unica (C3) are both highly reactive but have a significant slow component, which is consistent with the high variability of the hydrological functioning described by the class. Canamero (C4) has no highly reactive functioning but a significant slow component, thus corresponding to the low variability of hydrological functioning of the class. On the other hand, Gato Cave (C4) seems to be more reactive but still has a considerable slow component. Gato Cave is very close to the threshold of the C3 class (3%), which would indicate a medium variability of the hydrological functioning. Vacelliera and Zaghouan (C6) are both very inertial with low variability of the hydrological functioning.

7 Precipitation-Discharge modelling

7.1 Model structure

We first approached the structure of the model with the help of expert knowledge from previous studies and preliminary analyses of precipitation and discharge. For each site, we looked into the major features that drive the functioning of the system and we associated the corresponding conceptual modelling (Table 3). We then modified this base structure according to modelling performance while trying to keep physical realism.

Table 3: Known system feature on each system based on previous expert knowledge and preliminary analyses of precipitation and discharge.

Known system feature	Conceptual modelling
Fast response with a network of conduits	Reservoir C with fast transfer function
Low porosity matrix	Reservoir M with slow transfer function
Matrix-conduits exchanges	Exchange function between M & C reservoirs
Overflow springs	Transfer function outside of the model
Hysteresis functioning	Hysteresis transfer function to C or S reservoirs

Figure 9 presents the most efficient model structure that we obtained after performing modelling. The structure are based on (i) modelling performance, (ii) current knowledge of the system, and (iii) results from the preliminary analyses of discharge and precipitation.

Lez spring (Figure 9a) discharge exhibit slow and rapid flow components as well as matrix-conduits exchanges. The soil over the catchment is very shallow thus we considered a low soil available water capacity. The discharge lost during activation of overflow springs was simulated with a function that transfers water outside of the model. Aubach system (Figure 9b) exhibit a very reactive response and a part of the discharge is lost through several overflow springs. The soil is very shallow so we did not consider a soil available water capacity. Vacelliera and Zaghouan systems (Figure 9c and 9h) hydrological functioning are not well known so model structure proposal is mainly based of the preliminary analyses. They both showed a very inertial functioning that indicates slow transfer through the system. Qachqouch spring (Figure 9d) discharge exhibit slow and rapid flow components as well as matrix-conduits exchanges. We considered a direct transfer function (Q_{ESO}) as the system has many different response times. Unica (Figure 9e) is a large and complex system that exhibit slow and rapid flow components, matrix-conduits exchanges, as well as hysteresis functioning. It also has overflow springs and is under influence of polje flooding during wet periods. However, we only retain a very simple structure with a slow compartment and a overflow direct transfer function. Canamero and Gato Cave systems (Figure 9f and 9g) have a similar model structure with slow and rapid flow components. The only differences are that we considered an overflow component for Canamero, and a low soil available water capacity for Gato cave.

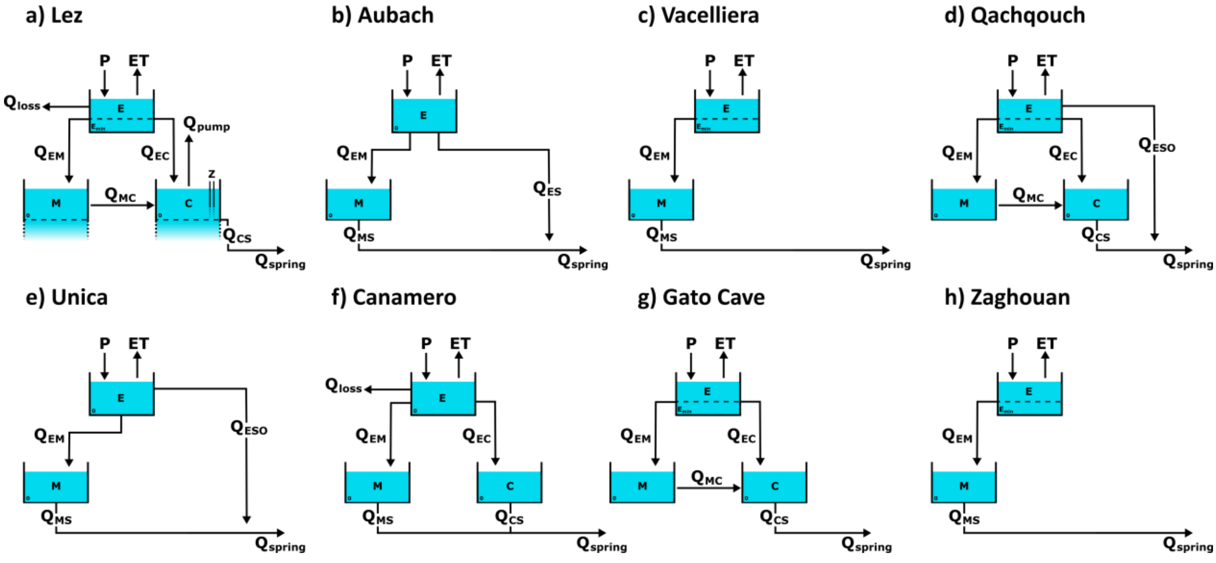

Figure 9: Most efficient model structures for each test site.

There is an interesting similarity between the classification of the system (section 6.1) and the model structure.

Qachqouch and Unica system are both classified C3 and have an overflow direct transfer function (Q_{ESO}). This fast flow component may be necessary to reproduce the highly reactive responses in some specific conditions, in relation to the identified high variability of hydrological functioning.

Canamero and Gato Cave are both classified C4 and have a standard model structure with a fast and slow component. As the systems are located in the same area, the similar hydrological functioning may be explained by similar lithology and karstification processes that occurred in the past.

Vacelliera and Zaghouan systems are both classified C6 and have a model structure with only a slow component. The C6 class contains karst systems with a very inertial and steady hydrological functioning, which is consistent with the retained structure that only allows slow flows through the M reservoir.

There is no evident relation between Lez and Aubach systems, even though they are both classified C2. It may be due to the anthropogenic influence on the Lez that necessarily impacts the hydrological functioning of the system. In fact, we can imagine that without pumping, the Lez system would have a more dampened response, resulting in a slower draining of the capacitive function (and lower α_{mean}). This would result in a C4 classification and the model structure would be consistent with those of Canamero (C4) and Gato Cave (C4) that is the standard slow and fast- components.

7.2 Modelling approach

Table 4 depicts the time intervals of the calibration and validation period for each site, associated with overview analyses: daily mean discharge (Q_{mean}), annual redistributed precipitation (rP_{an}, calculated from daily mean precipitation multiplied by 365) and daily mean evapotranspiration (ET_{mean}). The last column gives details about the objective function and the performance criteria that were used for the calibration of the model.

Table 4: Time intervals of the calibration and validation periods with (i) associated statistical analyses on discharge, redistributed precipitation and evapotranspiration; and (ii) objective function. Q stands for discharge and Z for piezometry.

System		Calibration period		Validation period		Objective function
		From	To	From	To	
Lez	Period	2008-10-21	2016-12-31	2017-01-01	2018-12-30	0.5NSE(Q)+0.5NSE(Z)
	Q_{mean} ($m^3.s^{-1}$)	0.87		1.05		
	rP_{an} (mm)	943		891		• NSE for Q > 0 $m^3.s^{-1}$
	ET_{mean} (mm)	1.23		1.18		• NSE for Z < 64.5 m
Aubach	Period	2014-04-18	2019-12-31	2020-01-01	2020-10-31	NSE(Q)
	Q_{mean} ($m^3.s^{-1}$)	0.88		1.15		
	rP_{an} (mm)	2061		2562		
	ET_{mean} (mm)	1.2		1.44		
Vacelliera	Period	2018-06-13	2020-03-24	2020-03-25	2020-09-21	NSE(Q)
	Q_{mean} ($m^3.s^{-1}$)	0.06		0.04		
	rP_{an} (mm)	1342		1088		
	ET_{mean} (mm)	1.12		2.06		
Qachqouch	Period	2015-09-06	2019-09-30	2019-10-01	2020-01-22	NSE(Q)
	Q_{mean} ($m^3.s^{-1}$)	1.94		2.83		
	rP_{an} (mm)	1189		2501		
	ET_{mean} (mm)	1.12		0.95		
Unica	Period	1961-01-02	2016-09-28	2016-09-29	2018-12-31	NSE(Q)
	Q_{mean} ($m^3.s^{-1}$)	21.85		24.91		
	rP_{an} (mm)	1604		1639		
	ET_{mean} (mm)	2.04		2.23		
Canamero	Period	2008-02-15	2009-08-18	2009-08-19	2010-05-13	NSE(Q)
	Q_{mean} ($m^3.s^{-1}$)	0.63		1.71		
	P_{an} (mm)	715		1628		
	ET_{mean} (mm)	4.12		3.61		
Gato Cave	Period	1963-10-02	2011-09-03	2011-09-04	2015-04-29	NSE(Q)

System		Calibration period		Validation period		Objective function
		From	To	From	To	
	Q_{mean} ($m^3.s^{-1}$)	1.48		1.79		
	P_{an} (mm)	1855		2091		
	ET_{mean} (mm)	2.98		2.95		
Zaghouan	Period	1915-07-20	1917-03-11	1917-03-12	1918-01-01	NSE(Q)
	Q_{mean} ($m^3.s^{-1}$)	0.1		0.11		
	P_{an} (mm)	547		372		
	ET_{mean} (mm)	2.36		2.96		

The validation period of Aubach, Qachqouch, Unica, Canamero and Gato Cave systems seems to be wetter than the calibration period, especially for Qachqouch and Canamero where the precipitation are estimated to be twice as much. On the other hand, the Lez, Vacelliera and Zaghouan systems had dryer meteorological regime on the validation period than the calibration period.

All systems except Vacelliera have increases in mean discharge in the validation period. Lez and Zaghouan system show this increase despite a lower annual redistributed precipitation. It can be related to the intra-annual distribution of the precipitation that is not fully caught with the calculation method of rP_{an}. The changes in discharge range from 10% to 171%. The evapotranspiration is higher during the validation period for Aubach, Vacelliera, Unica and Zaghouan systems, and is lower or equal for the other systems.

The calibration of the models was realized with the Nash-Sutcliffe Efficiency coefficient for all systems. For the Lez, we used a composite function of NSE over spring discharge and piezometry to consider the hydrological functioning in its totality. We calibrated the model over observed discharge when the discharge is greater than 0 m^3/s^{-1} and over piezometry when the spring is dry.

The results of the models were evaluated on validation periods that range between 4 and 44 months, depending on the length of the entire time series. We used 8 performance criteria to assess the performance of the models: NSE over (i) all discharges, (ii) low discharges, (iii) medium discharges, and (iv) high discharges; the 3 components of KGE (r, β and α); and BE. The high discharges threshold corresponds to the 0.9 quantile of the observed discharges and the low discharges threshold is equal to 0.4 time the mean of observed discharge.

We calculated a modified NSE criterion according to Mathevet et al. (2009). They proposed a bounded version of NSE that allows an easier comparison between different sites as well as different discharge states. The lower bound of the C2M criterion is equal to -1, thus allowing a better comparison of the results when very low performances occur, which can heavily influence comparisons in terms of mean NSE values.

$$C_{2M} = \frac{NSE}{2 - NSE}$$

The C_{2M} criterion is less optimistic than NSE (Figure 10) for values greater than 0.

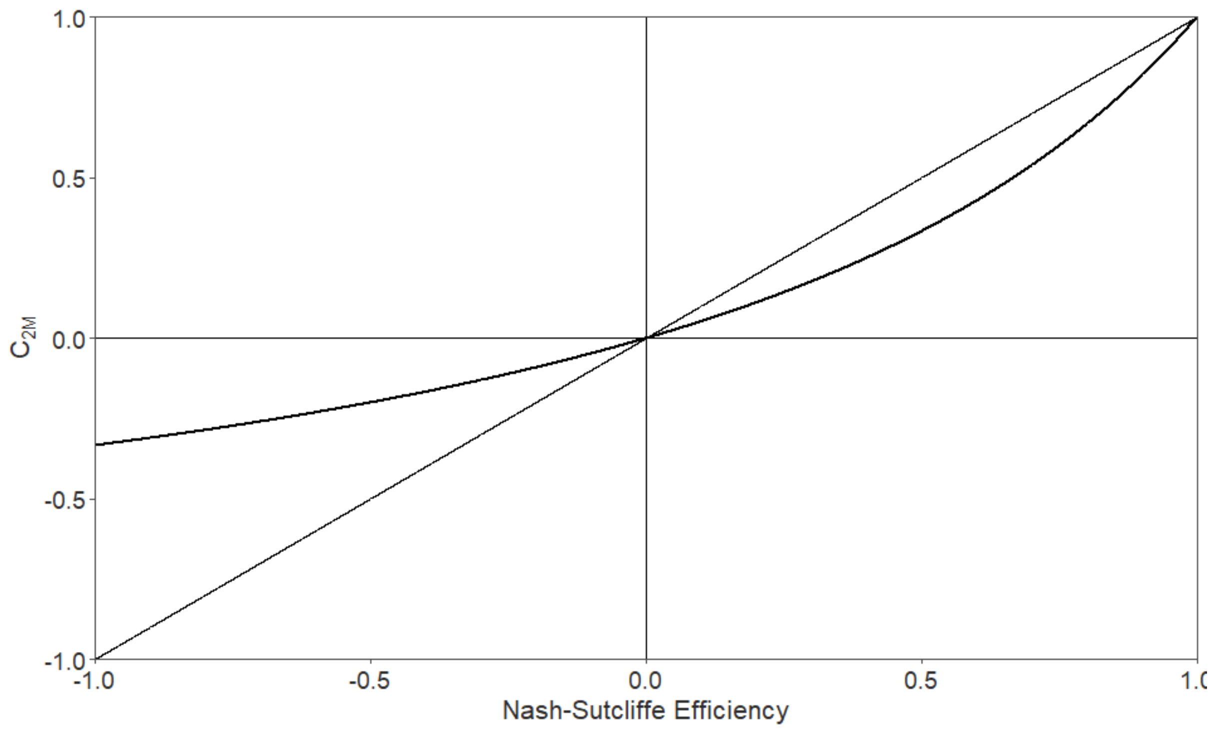

Figure 10: Relation between NSE and C_{2M} criteria (Mathevet et al., 2009).

7.3 Modelling results

7.3.1 Lez

The simulated discharges and piezometry are presented in Figure 11 for the calibration period, and in Figure 12 for the validation period. On the two periods, the results of the models are assessed with several performance criteria (Figure 13).

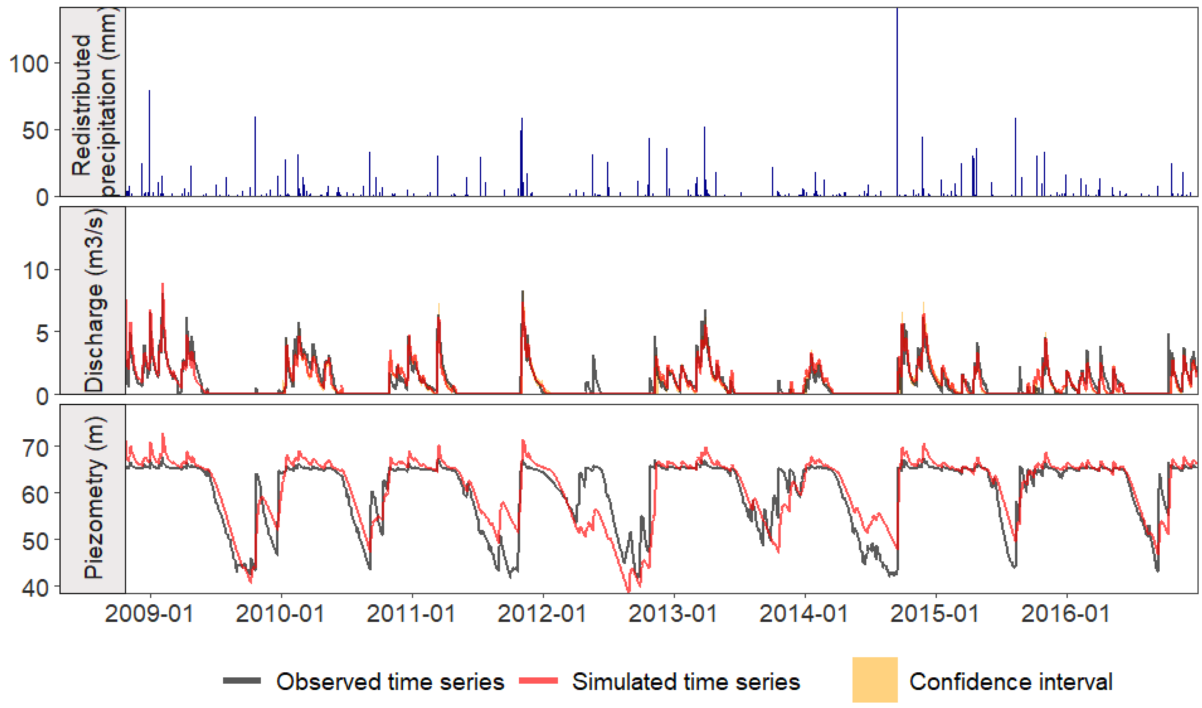

Figure 11: Observed and simulated Lez spring discharge time series (bottom) and redistributed precipitation (top) for the calibration period.

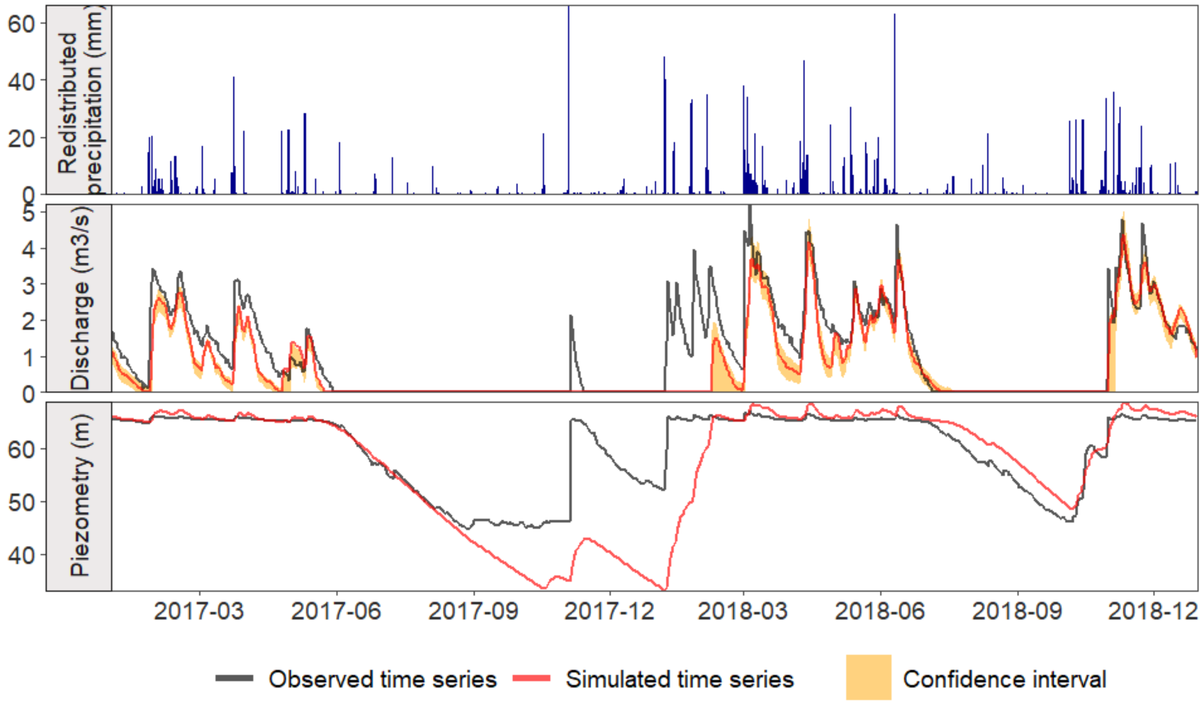

Figure 12: Observed and simulated Lez spring discharge time series (bottom) and redistributed precipitation (top) for the validation period.

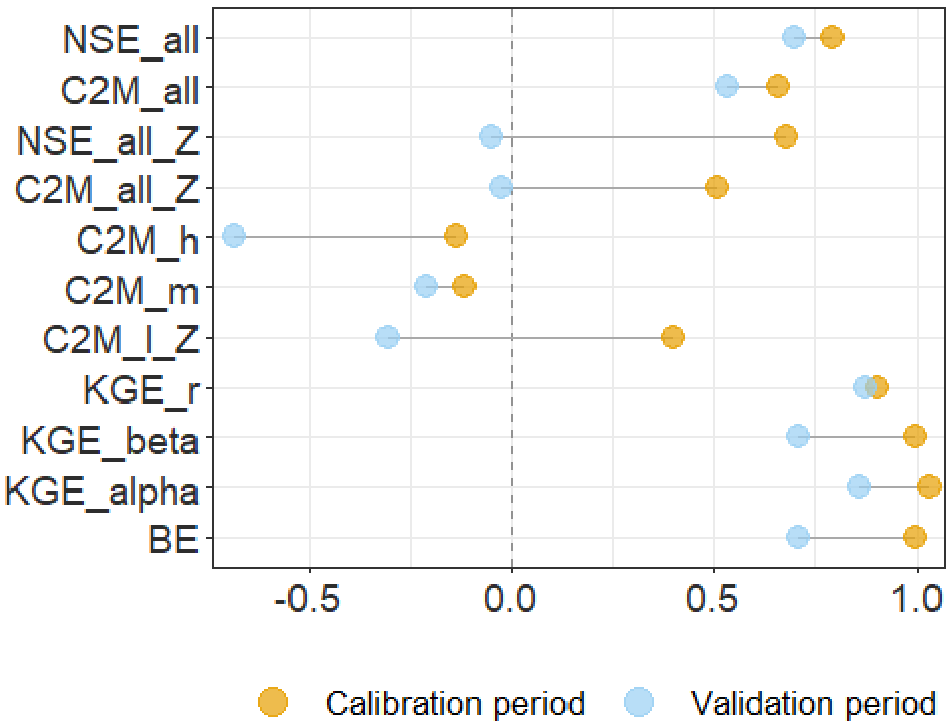

Figure 13: Comparison of the Lez model results through different performance measures on the calibration and validation periods.

On the calibration period, the model satisfactorily simulates both discharges (C_{2M}=0.657, NSE=0.793) and piezometry (C_{2M}=0.511, NSE=0.677). The overall dynamics are quite good, especially on flood peaks during wet periods. However, the model fails to accurately reproduce the first floods after or during the dry periods. This weakness can also be observed on the piezometric level time series, where the model does not succeed to reproduce the dynamics of draining and repletion of the capacitive part of the aquifer. It may be due to an unadapted soil available water capacity, or a significant hysteresis functioning that is not considered in the model.

On the validation period, the model shows lower performance on discharges (C_{2M}=0.536, NSE=0.698) and piezometry (C_{2M}=-0.024, NSE=-0.048). This difference is likely explained by a particular period between september 2017 and march 2018, where the observed piezometric level plateaus at around 47 m above sea level. As the model does not reproduce the plateau, there is a large error on the reservoir level that induces a high delay in the spring response. Several boreholes at the north of the spring showed flow-bearing structures at 50 m above sea level (Dausse et al., 2019). These fast water transfer are not considered in the model and could explain the fast increases of piezometric level and reactive spring responses. We also suspect an evolution of the carbonates facies with depth, which could affect the effective porosity of the media and induce different flow dynamics.

The KGE components indicate a satisfying shape and timing in both calibration (r=0.9) and validation (r=0.87), and very good estimations of discharged volumes (β=1) and flow variability (α=1.03) in calibration. There is a deficit in discharged volumes (β=0.71) and less flow variability (α=0.86) regarding the observed time series in the validation period. The reservoir without bottom that cannot reproduce the observed piezometry level likely induces a loss in water.

Lez system modelling is challenging because of the continuous pumping into the saturated zone of the aquifer. This anthropogenic forcing induces a huge decrease of the piezometric level during summer and causes the spring to dries out. Still, the model is satisfactory and can nicely reproduce the overall dynamics of the system. The main aspects of the precipitation-discharge relationship that the model struggles to reproduce are (i) reservoir levels during dry periods, and (ii) first floods after or during dry periods. These aspects can be investigated by studying (i) the soil available water capacity, (ii) a potential hysteresis functioning, (iii) an evolution of the carbonate facies with depth, or (iv) the importance of the preferential water path a high depth.

7.3.2 Aubach

The simulated discharges are presented in Figure 14 for the calibration period, and in Figure 15 for the validation period. On the two periods, the results of the models are assessed with several performance criteria (Figure 16).

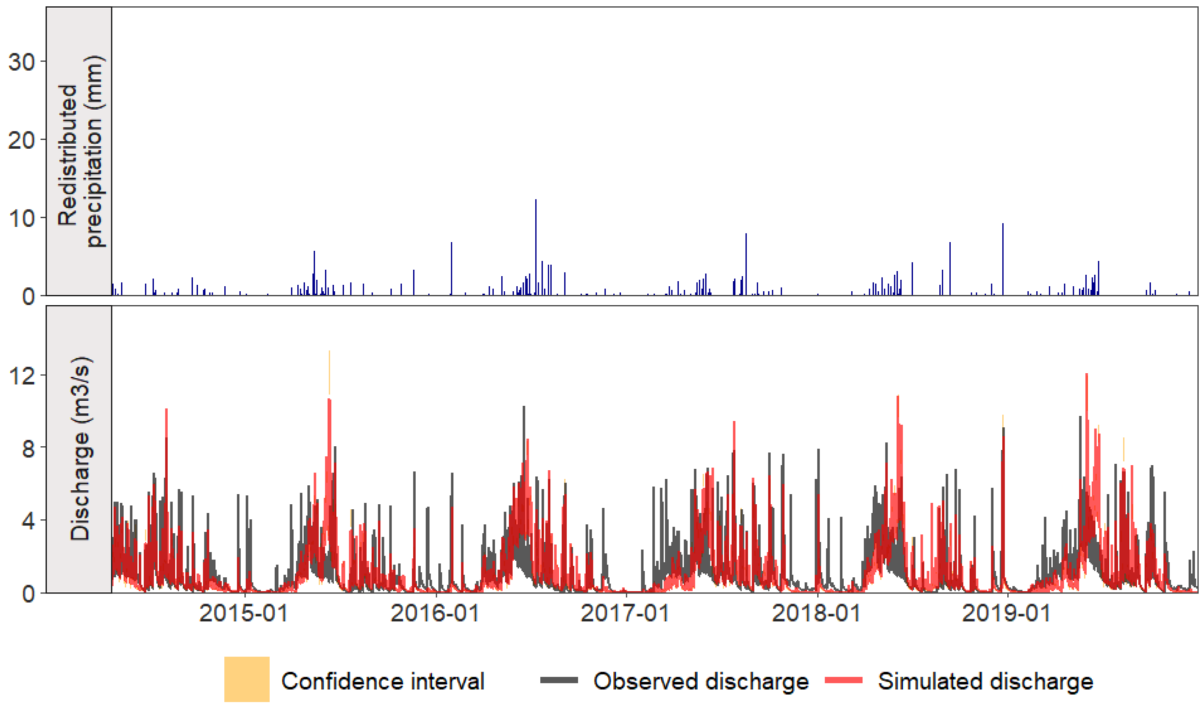

Figure 14: Observed and simulated Aubach spring discharge time series (bottom) and redistributed precipitation (top) for the calibration period.

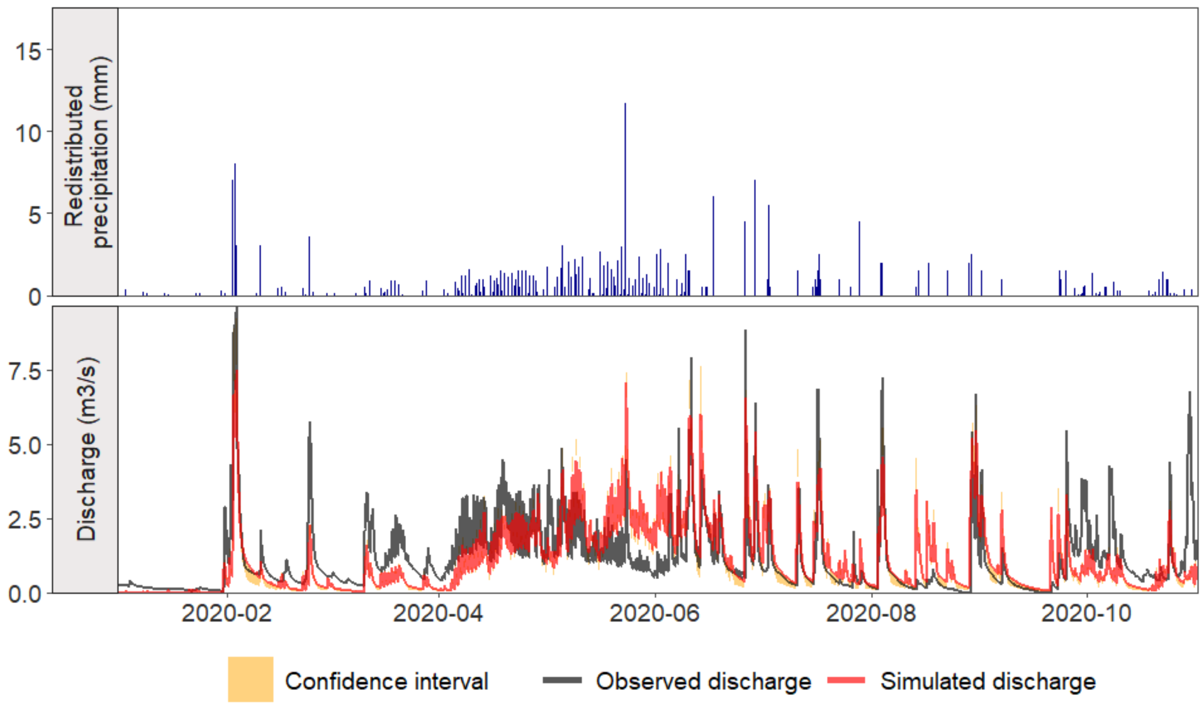

Figure 15: Observed and simulated Aubach spring discharge time series (bottom) and redistributed precipitation (top) for the validation period.

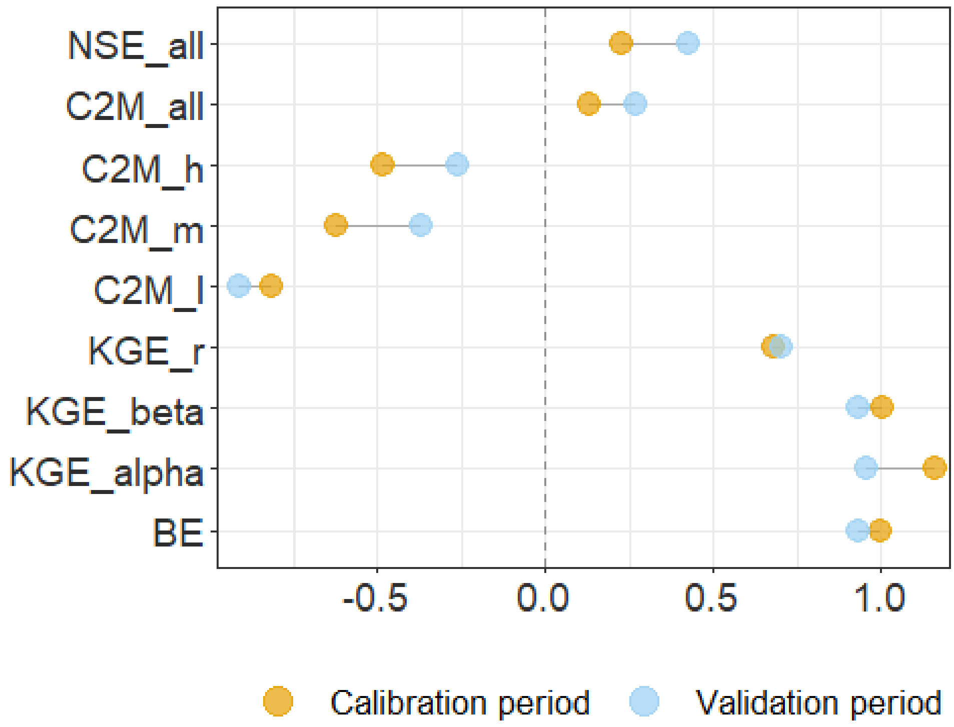

Figure 16: Comparison of the Aubach model results through different performance measures on the calibration and validation periods.

On the calibration period, the model is not satisfactory with a C_{2M} of 0.13 and NSE of 0.23. The overall dynamics are quite good but the model fails to accurately reproduce the discharges during winter and spring seasons. There is a consistent deficit in water during winter/early spring and an excess during late spring. It is likely due to a miscalibration of the snow routine, retaining too much water as snow in winter and thus releasing too much in warmer periods. We can also appreciate that some flood events in cold periods are not reproduced at all due to the lack of precipitation input.

The results are a bit better on the validation period (C_{2M}=0.27, NSE=0.425), which are likely due to a lower error of the redistributed precipitation input for this year.

The KGE components indicate a bad shape and timing (r) and very good estimations of discharged volumes (β) in both calibration (r=0.68 and β=1) and validation (r=0.7 and β=0.93). There is too much flow variability in the calibration period (α=1.16). The low r and high α values are likely related with the miscalibration of the redistributed precipitation input, that induces a shift in the overall flow dynamics and may bring too much water in one go in the upper reservoir, thus inducing very high flood peaks.

Aubach system is challenging because of the high differences in altitude and heterogeneity of precipitation. This makes it difficult to provide accurate inputs for the model, especially regarding snow dynamics. Setting apart the mismatches related to inadequate meteorological inputs, the model structure seems appropriate to simulate the hydrological response of the spring. The reactive component of the system is reproduced through the Q_{ES} transfer function while the slow depletion of the capacitive part is simulated with the matrix reservoir. We also tested different configurations (lost discharge from upper level reservoir and/or pumping in lower reservoirs) to simulate the lost discharges through overflow springs and underground flows, but there were no significant increases in model performance.

7.3.3 Vacelliera

The simulated discharges are presented in Figure 17 for the calibration period, and in Figure 18 for the validation period. On the two periods, the results of the models are assessed with several performance criteria (Figure 19).

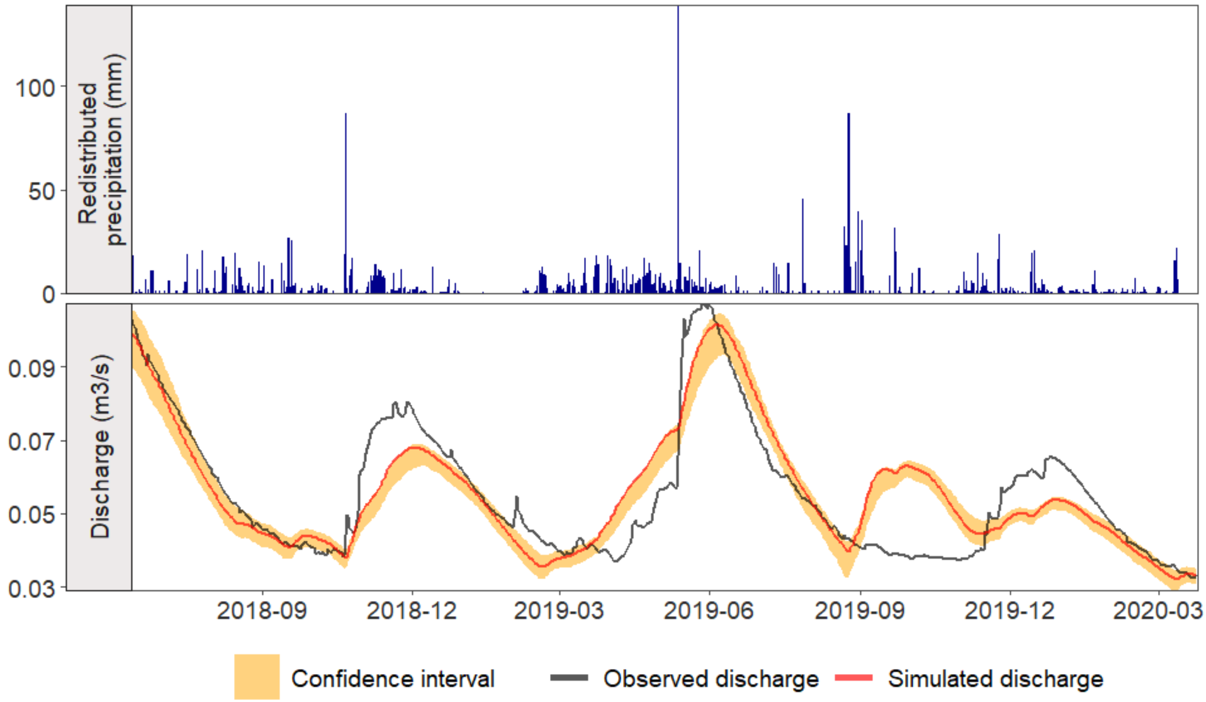

Figure 17: Observed and simulated Vacelliera spring discharge time series (bottom) and redistributed precipitation (top) for the calibration period.

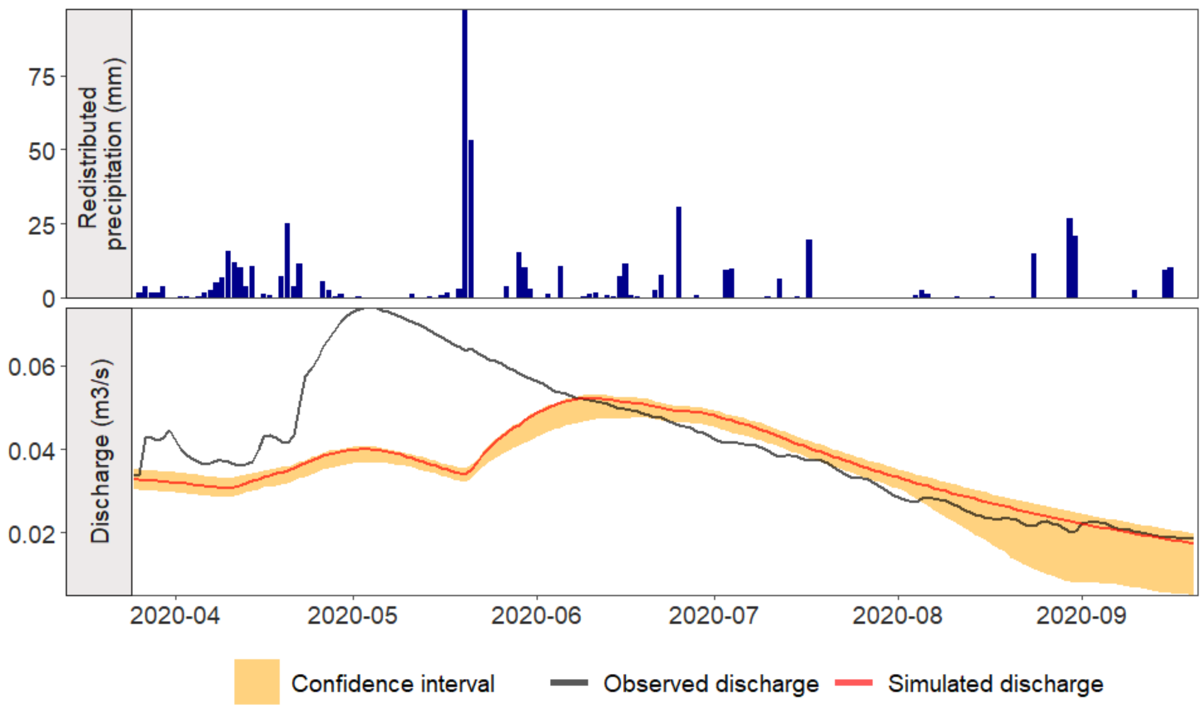

Figure 18: Observed and simulated Vacelliera spring discharge time series (bottom) and redistributed precipitation (top) for the validation period.

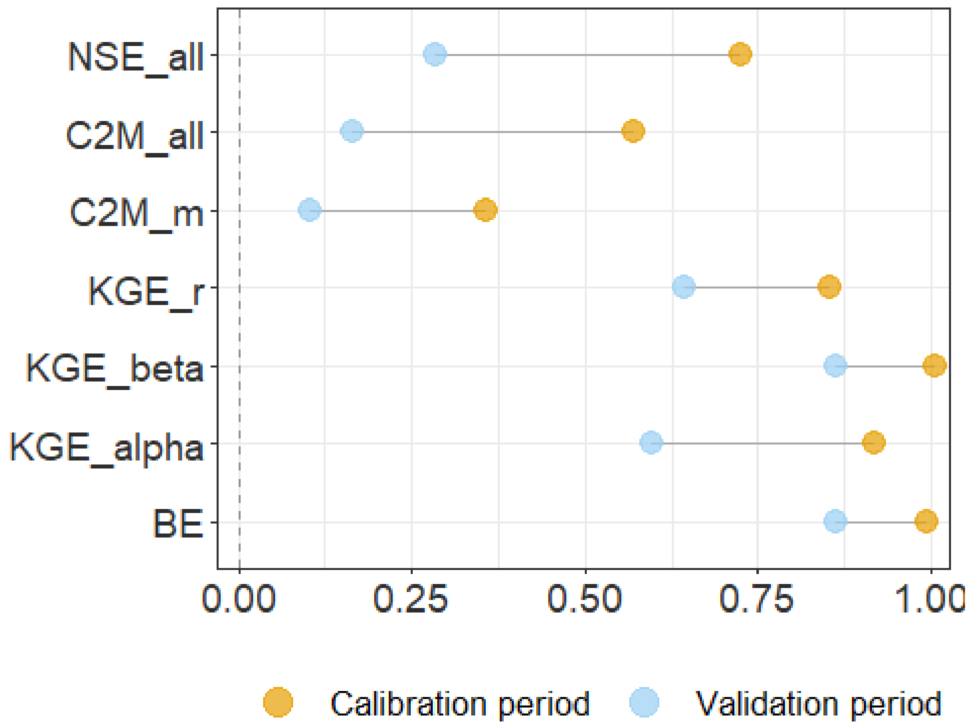

Figure 19: Comparison of the Vacelliera model results through different performance measures on the calibration and validation periods.

On the calibration period, the results are satisfactory with a C_{2M} of 0.57 and NSE of 0.726. The overall inertial dynamics are caught by the model. In September 2019, a recharge event occurs but does not influence observed discharges. However, it induces a large error as the model simulates a response at the spring. It is likely due to a miscalibration of the snow routine or wrong assessment of the precipitation, as we can see a deficit in water months after the event.

The results are worse on the validation period (C_{2M}=0.165, NSE=0.284). This high difference can be easily explained by the precipitation input, where the precipitation on 2020-05-20 and 2020-05-21 only produced a negligible increase. It may be a limitation due to the mountainous aspect of this system as the meteorological station is located on the other side of the massif.

Although the KGE components are quite good in calibration period (r=0.85, β=1.01 and α=0.92), there is a high diminution of their values in the validation period (r=0.64, β=0.86 and α=0.6). It is likely related to the redistributed precipitation input, which can explain the errors in shape and timing, as well as flow variability.

The absence of a fast transfer function in the model structure indicate that the karstification is low or very low. The soil available water capacity parameter increases the performance of the model and may translate slow infiltration processes through a poorly transmissive media. The overall dynamics are correct and the model succeed to reproduce the very inertial hydrological response of the system. The model can probably be improved with more accurate precipitation input, but it remains challenging due to the mountainous and snow problems.

7.3.4 Qachqouch

The simulated discharges are presented in Figure 20 for the calibration period, and in Figure 21 for the validation period. On the two periods, the results of the models are assessed with several performance criteria (Figure 22).

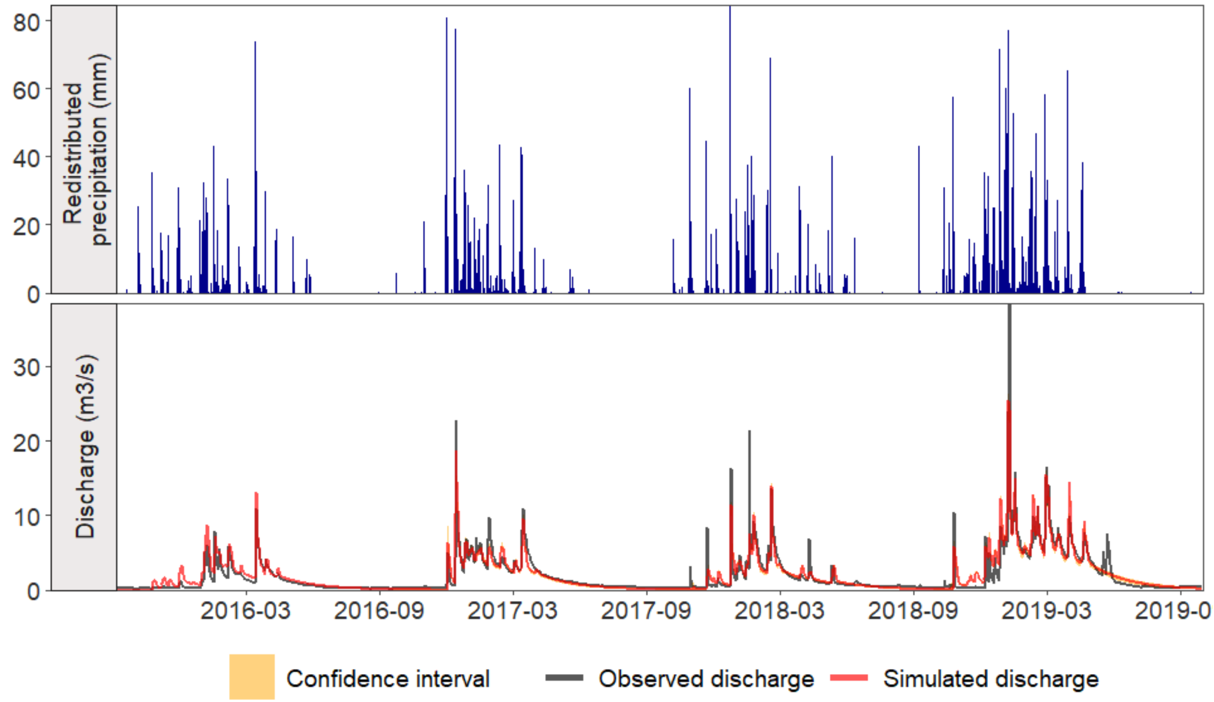

Figure 20: Observed and simulated Qachqouch spring discharge time series (bottom) and redistributed precipitation (top) for the calibration period.

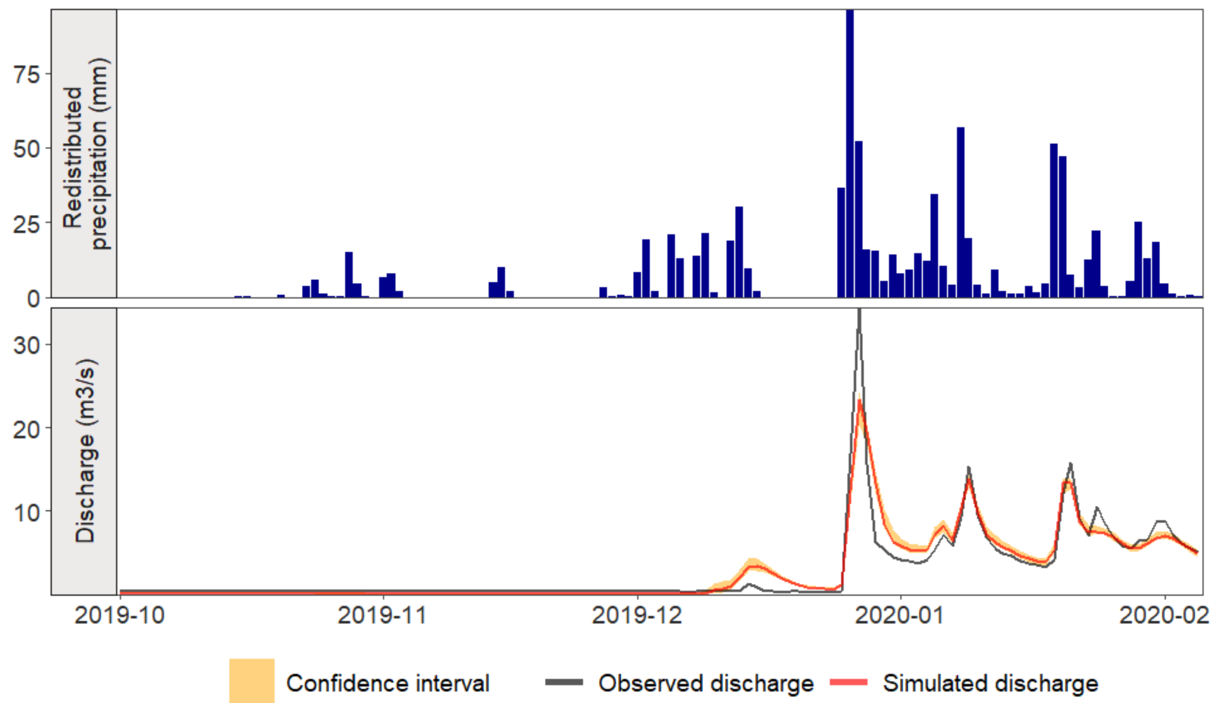

Figure 21: Observed and simulated Qachqouch spring discharge time series (bottom) and redistributed precipitation (top) for the validation period.

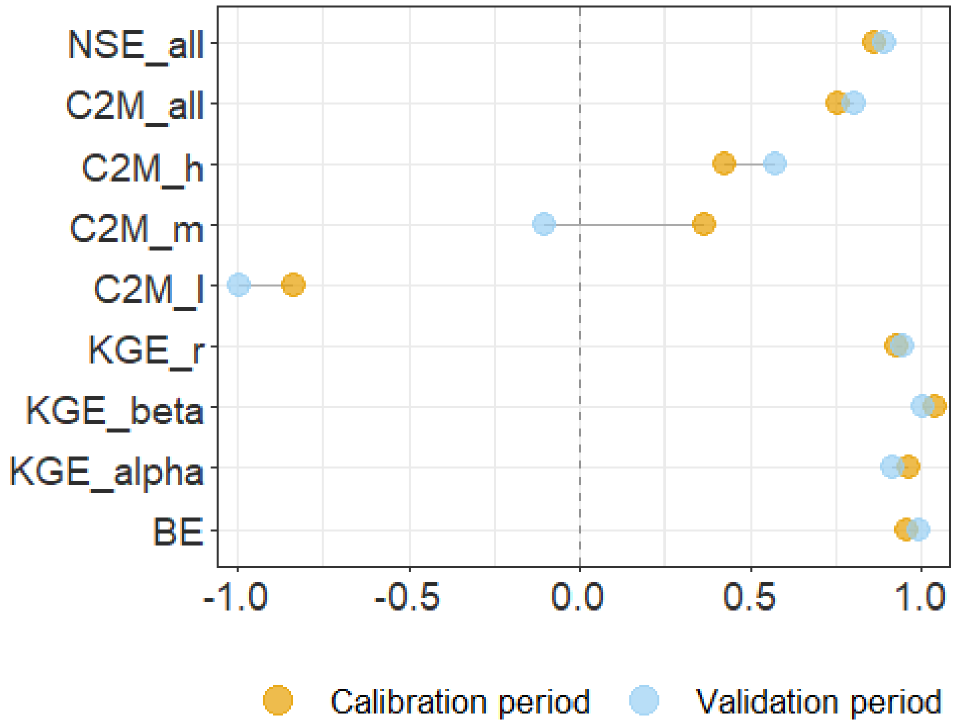

Figure 22: Comparison of the Qachqouch model results through different performance measures on the calibration and validation periods.

The model results are really good on both calibration (C_{2M}=0.753, NSE=0.859) and validation (C_{2M}=0.804, NSE=0.891) periods. The simulated dynamics are consistent with the observed hydrological response. However, the model struggles to reproduce very high flood peaks, which may be because of (i) inflows into the system that are not considered in the model, (ii) uncertainties on ungauged discharges and/or precipitation, or (iii) heterogeneity of precipitation. The model also often overestimates or underestimates flood events after dry periods, which is either (i) due a hysteresis functioning that is not considered, or (ii) a consequence of the soil available water capacity (E_{min}) that may be not representative of the whole catchment. However, E_{min} appeared to be critical for a satisfying modelling of low flows.

The KGE components are very good on both calibration period (r=0.93, β=1.04 and α=0.96) and validation period (r=0.94, β=1.01 and α=0.91). The β values higher than 1 suggest that there may be a little too much water in the model. The α values lower than 1 are likely related with the difficulties to reproduce high flood peaks.

The model structure highlights the presence of multiple flow components: (i) a very fast transfer function (Q_{ESO}), (ii) a fast transfer function corresponding to fractures and conduits (Q_{CS}), and (iii) a slow transfer function corresponding to matrix (Q_{MC}). The need for different speeds of water transfer indicate a highly hierarchized functioning of the system, which may be related to the shape of the catchment. The model has very good results and further performance enhancement may be achieved by working on the input data or by identifying specific functioning of the system.

7.3.5 Unica

The simulated discharges are presented in Figure 23 for the calibration period, and in Figure 24 for the validation period. On the two periods, the results of the models are assessed with several performance criteria (Figure 25).

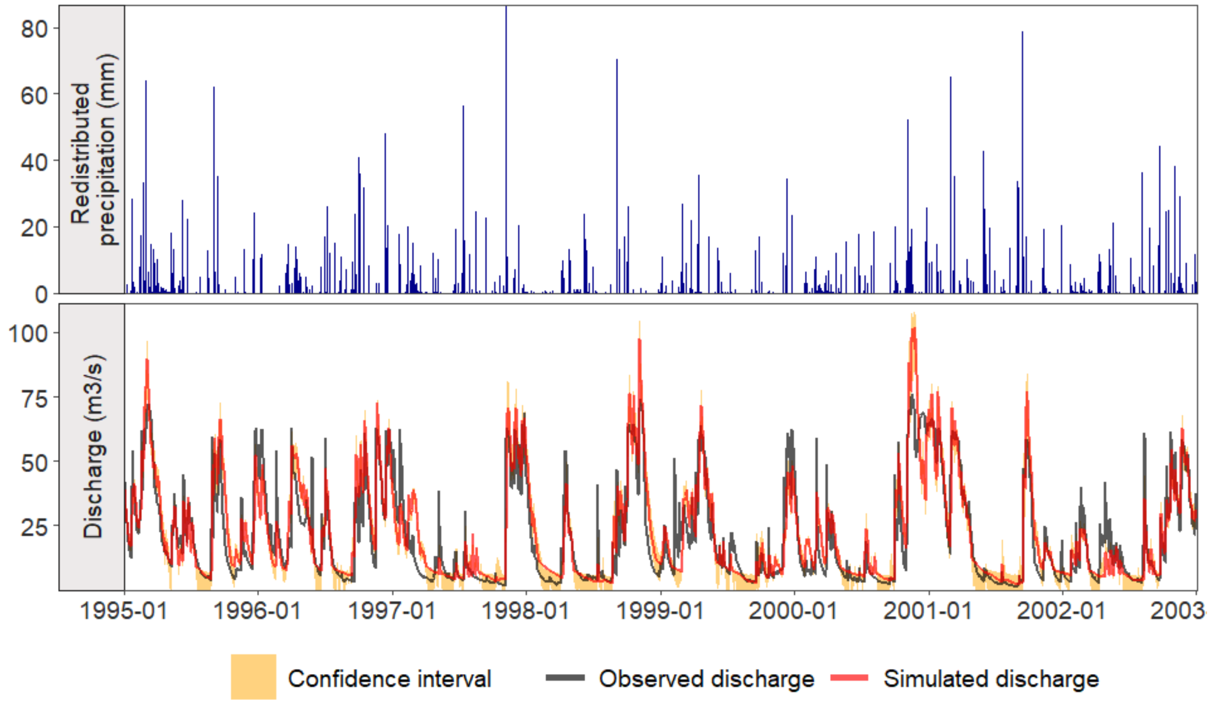

Figure 23: Extract of the observed and simulated Unica spring discharge time series (bottom) and redistributed precipitation (top) for the validation period.

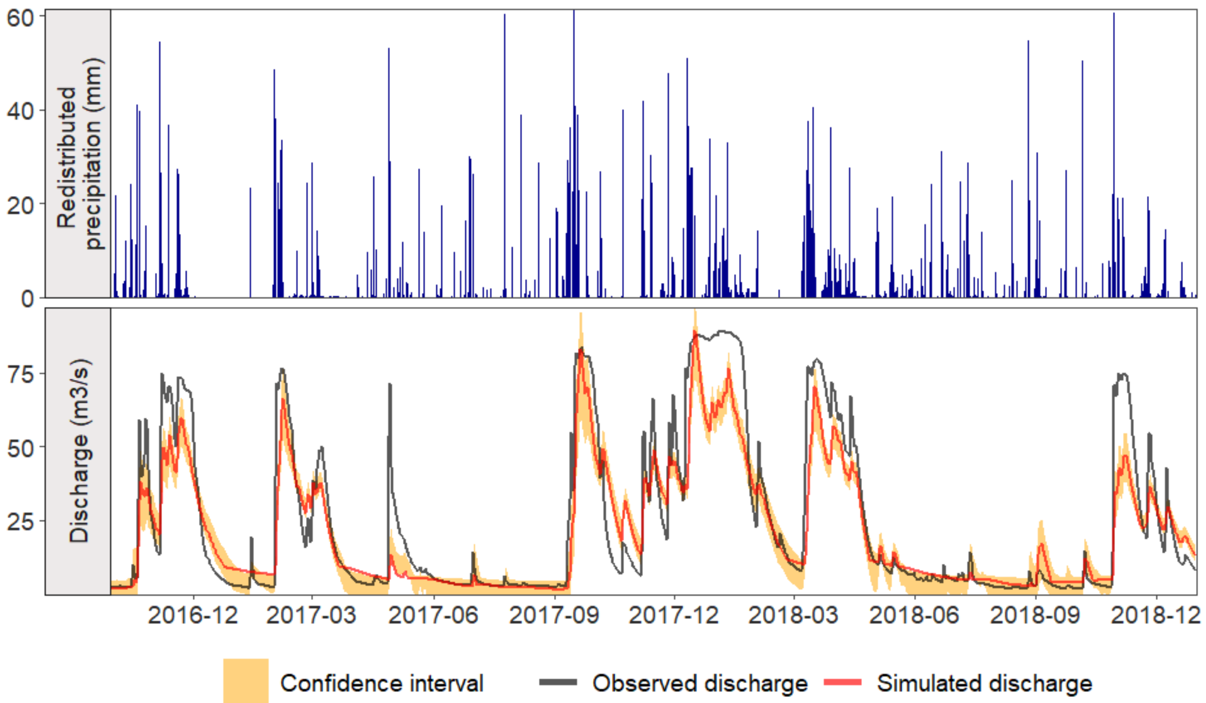

Figure 24: Observed and simulated Unica spring discharge time series (bottom) and redistributed precipitation (top) for the validation period.

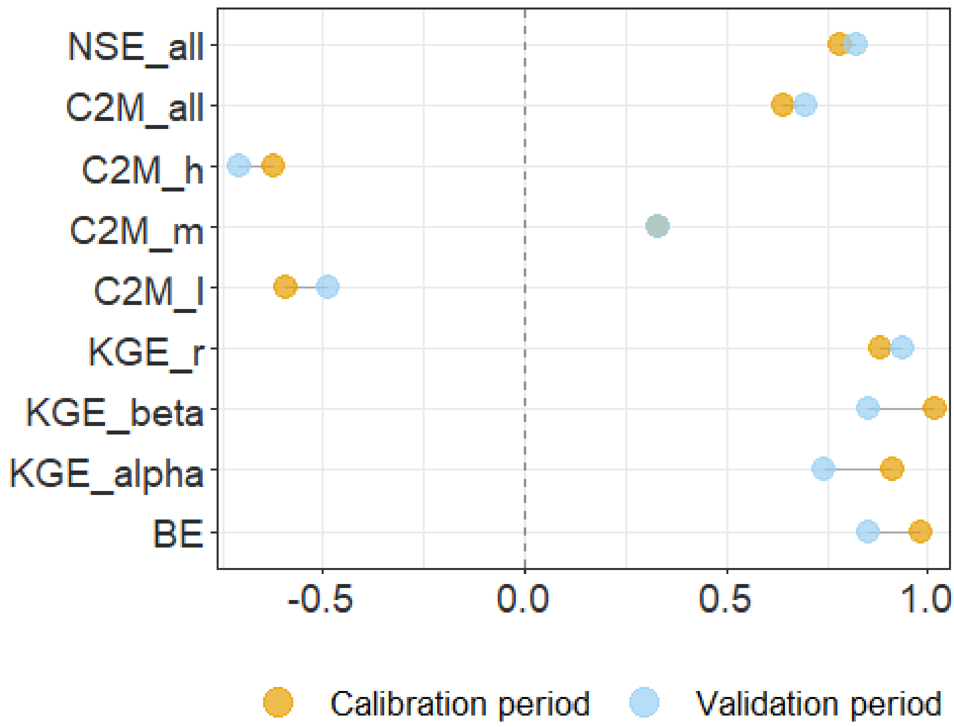

Figure 25: Comparison of the Unica model results through different performance measures on the calibration and validation periods.

The results are quite good on both calibration and validation periods with C_{2M} of 0.641, NSE of 0.781 and C_{2M} of 0.697, NSE of 0.822, respectively. The overall dynamics are relevant although there are inconsistencies during winter and spring seasons, likely due to snow melt that is not correctly simulated. The model also has difficulties to reproduce the depletion of the capacitive function, although a lot of different configuration have been tested. It may be due to the size and complexity of the catchment and due to very specific influence of poljes draining over the catchment, which cannot be simulated within KarstMod platform. The model also underestimates high discharge conditions and could not reproduce the plateau-like behaviours observed at very high discharge rates, which are due to the flood of a polje at Unica spring that influences the monitoring station.

The KGE components indicate a satisfying shape and timing in both calibration (r=0.88) and validation (r=0.94), and good estimations of discharged volumes (β=1.02) and flow variability (α=0.91) in calibration. There is a deficit in discharged volumes (β=0.85) and less flow variability (α=0.74) regarding the observed time series in the validation period (2016-2018). These differences may be related with the changes in land cover and recharge conditions (large-scale forest disturbance in the catchment), which happened between 2014 and 2018.

The retained model structure is pretty simple regarding this large complex system, but no other configuration was worth enough in terms of performance to be kept. It indicates that the system has a highly reactive response and a slow draining of the capacitive functioning that can be to a lesser extent related to the porous matrix of the aquifer and to a greater extent to the draining of the poljes. The model has good results and could benefit from more refined input data, although it is quite difficult regarding very large and complex catchment area. The consideration of the polje influence (as well as surface flow) may also increase the performance of the model.

7.3.6 Canamero

The simulated discharges are presented in Figure 26 for the calibration period, and in Figure 27 for the validation period. On the two periods, the results of the models are assessed with several performance criteria (Figure 28).

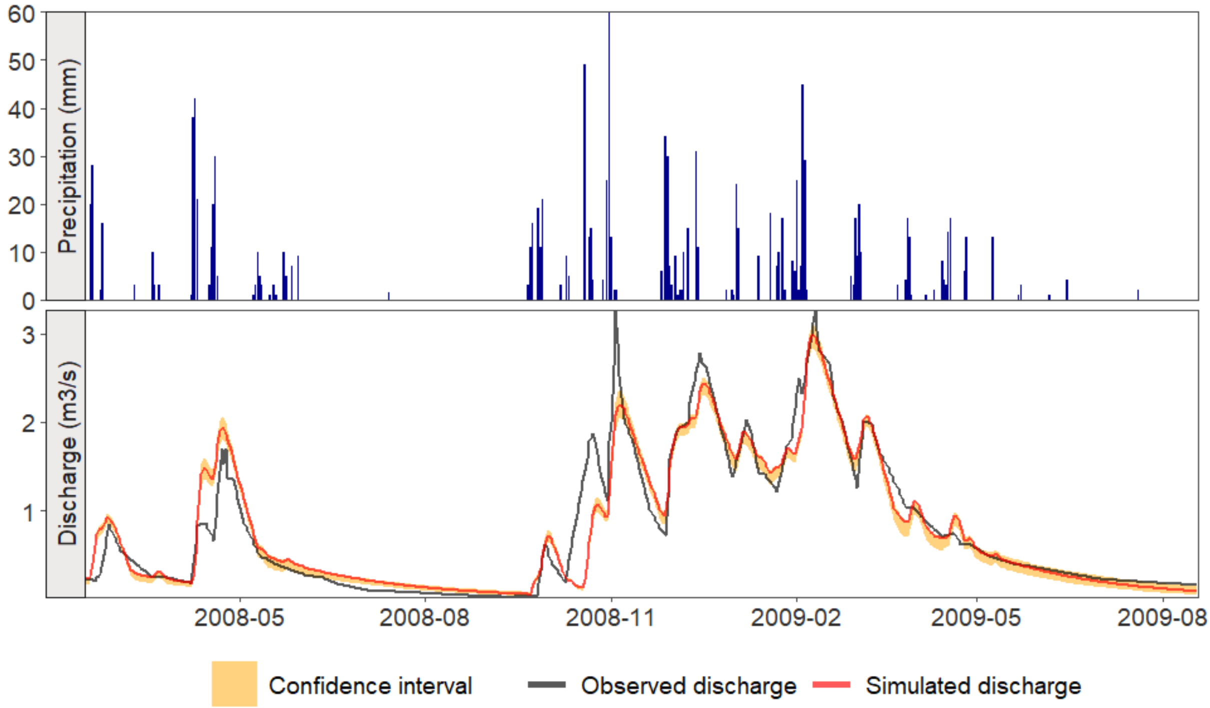

Figure 26: Observed and simulated Canamero spring discharge time series (bottom) and precipitation (top) for the calibration period.

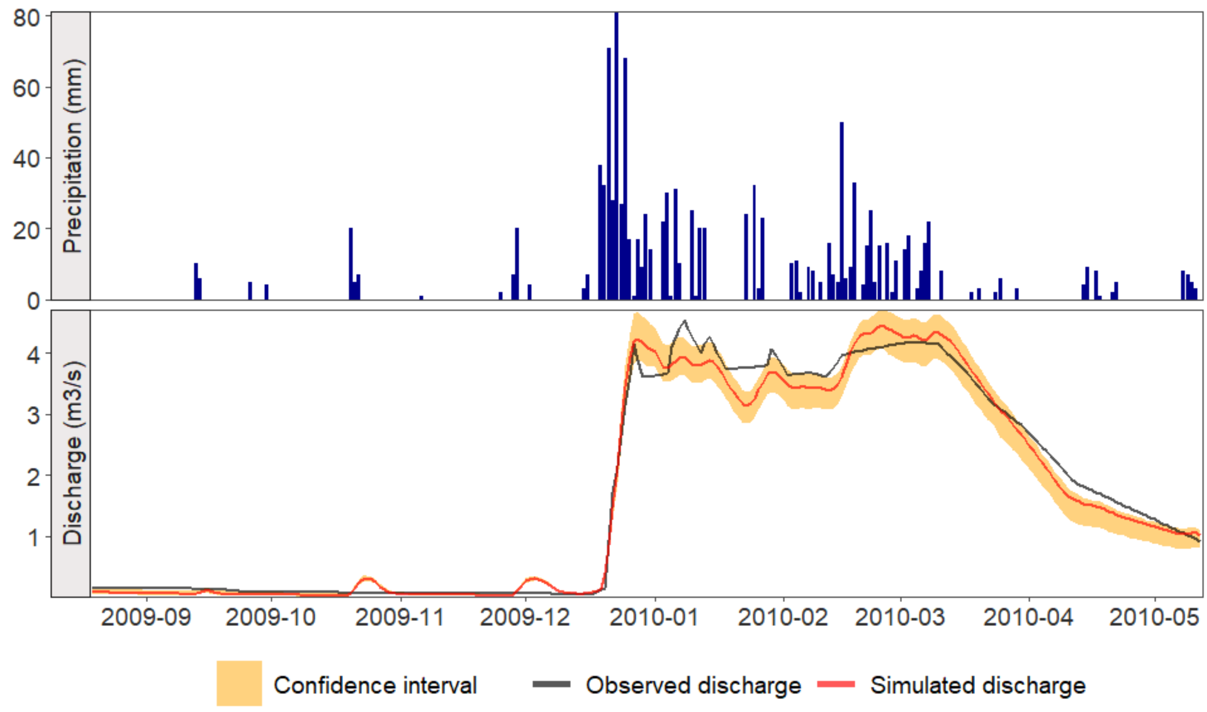

Figure 27: Observed and simulated Canamero spring discharge time series (bottom) and precipitation (top) for the validation period.

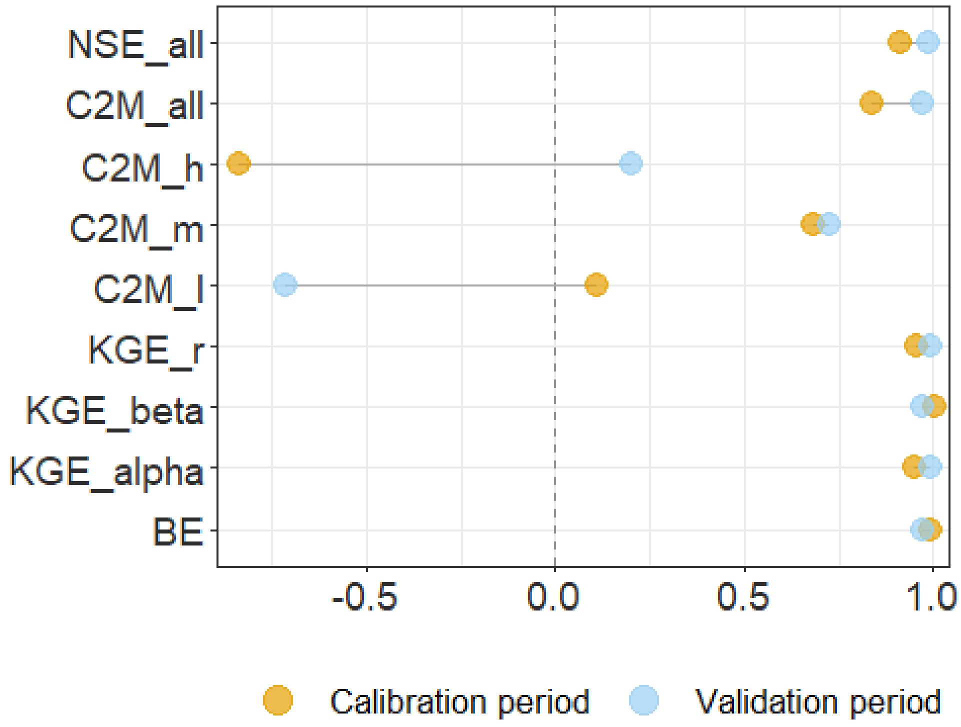

Figure 28: Comparison of the Canamero model results through different performance measures on the calibration and validation periods.

The results are very good on both calibration and validation periods with C_{2M} of 0.838, NSE of 0.912 and C_{2M} of 0.972, NSE of 0.986, respectively. The overall dynamics of the simulated discharge fit really well the observed time series. The imprecision of the model is likely due to uncertainties on the meteorological inputs and specific hydrological functioning of the system like localized recharge or occasional preferential flow paths that are not considered in the model structure.

The KGE components are very good on both calibration period (r=0.96, β=1.01 and α=0.95) and validation period (r=0.99, β=0.97 and α=0.99). The lower α in calibration period is explained by the struggle of the model to nicely reproduce the flood events of November 2018.

The two lower level reservoirs of the model correspond to a classical configuration of a karst system with a fast response through conduits and fractures and a slow response through matrix. The lost transfer function (Q_{loss}) was necessary to increase the performance of the model, which is consistent with the knowledge of several overflow springs on the catchment. The model has very good performance and we do not see any room for further improvement, other than having a longer time series to study different hydrological conditions.

7.3.7 Gato Cave

The simulated discharges are presented in Figure 29 for the calibration period, and in Figure 30 for the validation period. On the two periods, the results of the models are assessed with several performance criteria (Figure 31).

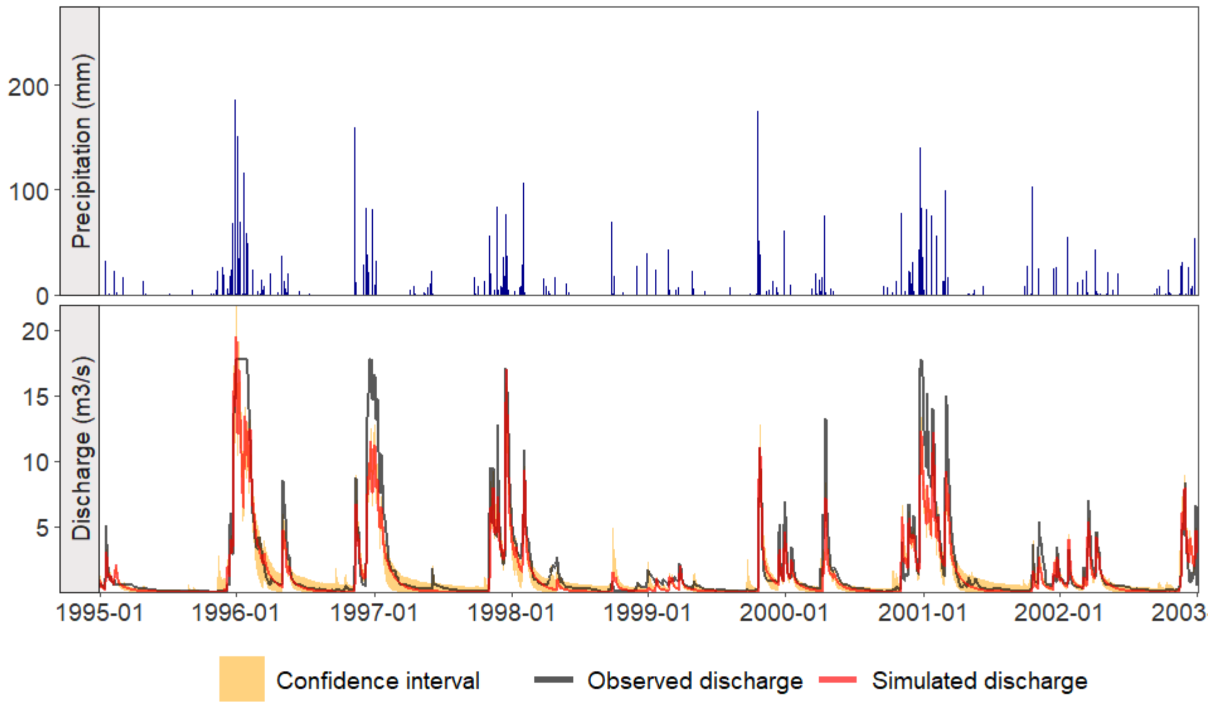

Figure 29: Extract of the observed and simulated Gato cave spring discharge time series (bottom) and precipitation (top) for the calibration period.

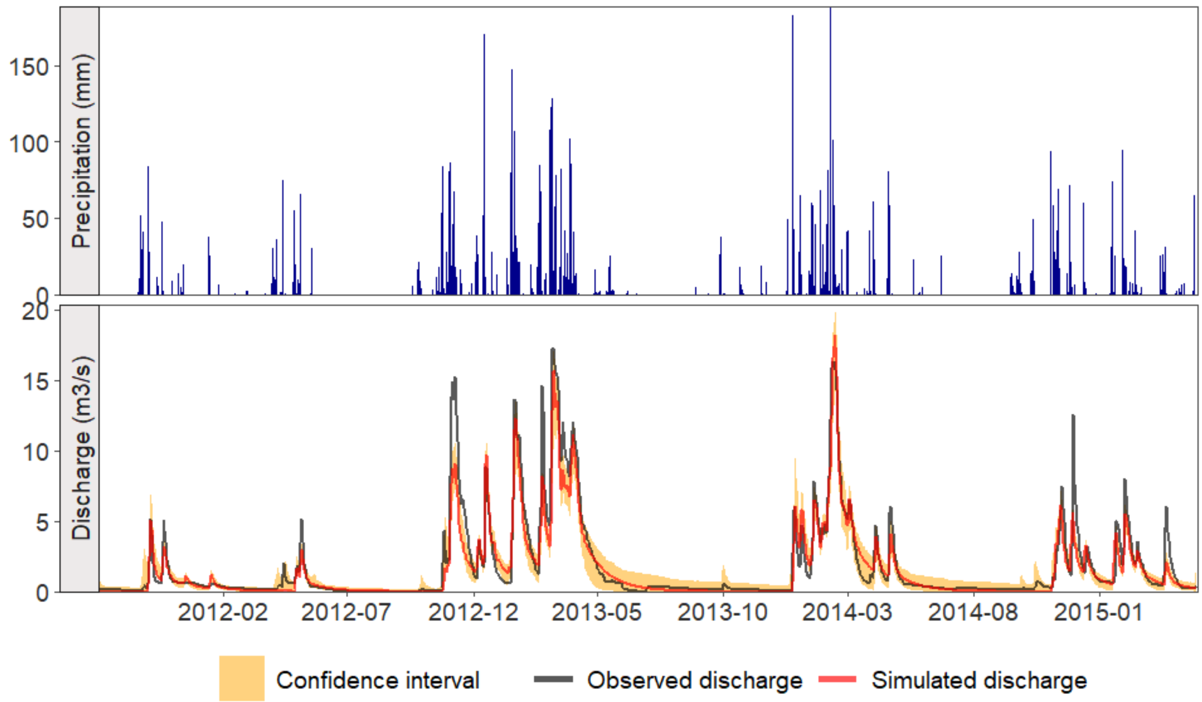

Figure 30: Observed and simulated Gato cave spring discharge time series (bottom) and precipitation (top) for the validation period.

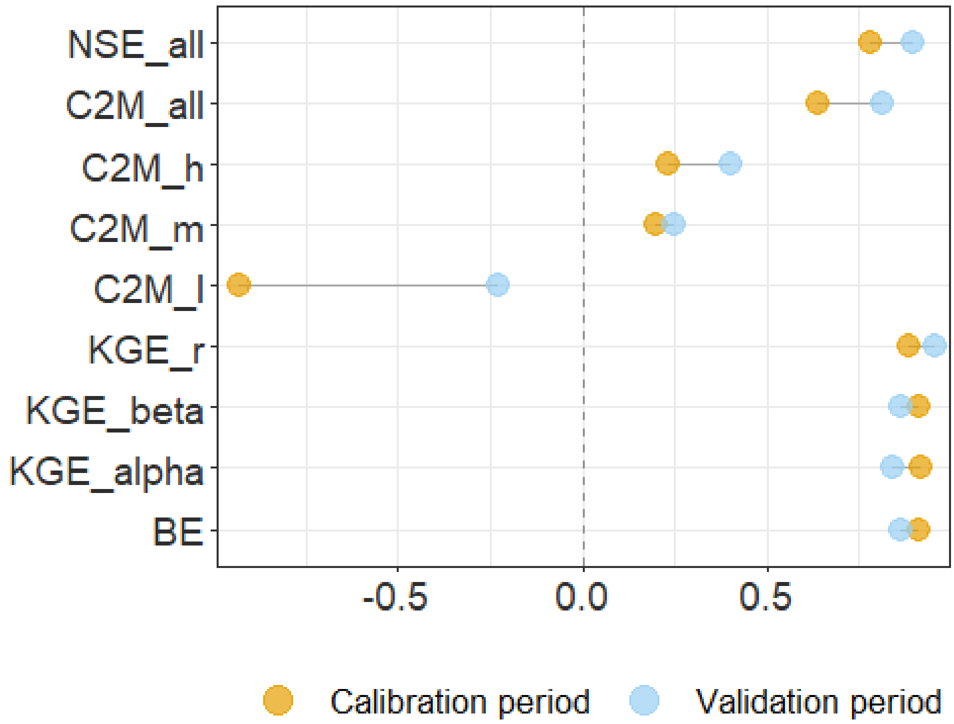

Figure 31: Comparison of the Gato Cave model results through different performance measures on the calibration and validation periods.

The results are quite good on both calibration and validation periods with C_{2M} of 0.638, NSE of 0.779 and C_{2M} of 0.813, NSE of 0.897, respectively. The overall dynamics of the simulated discharge are good although the model has difficulties to reproduce some high flows events. It seems to happen only when precipitation occur during several days without attaining really high values (e.g. 1997-01-01), which may indicate either (i) some kind of hysteresis functioning with flow occurring after established connection in the system, or (ii) inflows into the system that are not considered in the model. We tried to work with hysteresis transfer function but did not succeed in a better modelling of the observed discharges. The soil availability water capacity parameter (E_{min}) was necessary to correctly reproduce the discharge during dry periods, as there are many precipitation events that do not induce discharge at the spring.

The KGE components are good on both calibration period (r=0.88, β=0.91 and α=0.92) and validation period (r=0.96, β=0.86 and α=0.84). The model struggles to reproduce some flood peaks during the validation period, thus inducing a slight diminution of β and α. However, the higher r indicates a better catch on the shape and timing of the flow.

The classical model structure with a fast response through conduits and fractures and a slow response through matrix is sufficient to correctly simulate the discharge of Gato Cave spring, but the consideration of other internal processes could help to increase the performance of the model.

7.3.8 Zaghouan

The simulated discharges are presented in Figure 32 for the calibration period, and in Figure 33 for the validation period. On the two periods, the results of the models are assessed with several performance criteria (Figure 34).

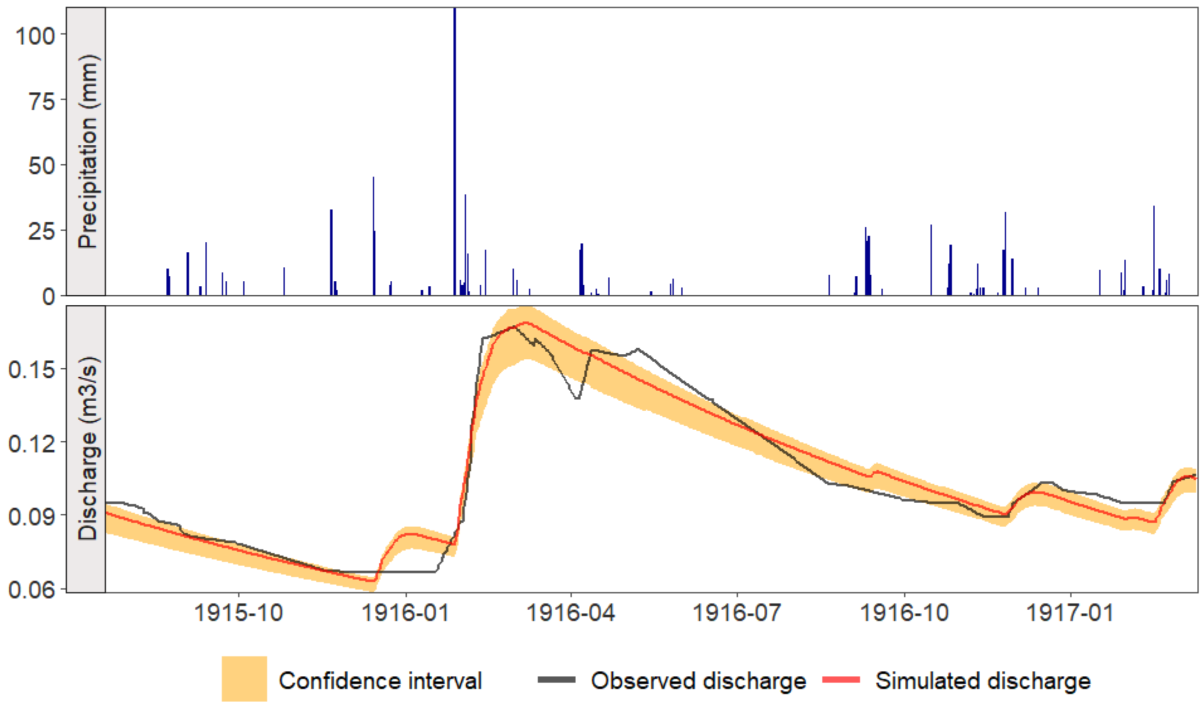

Figure 32: Observed and simulated Zaghouan spring discharge time series (bottom) and precipitation (top) for the calibration period.

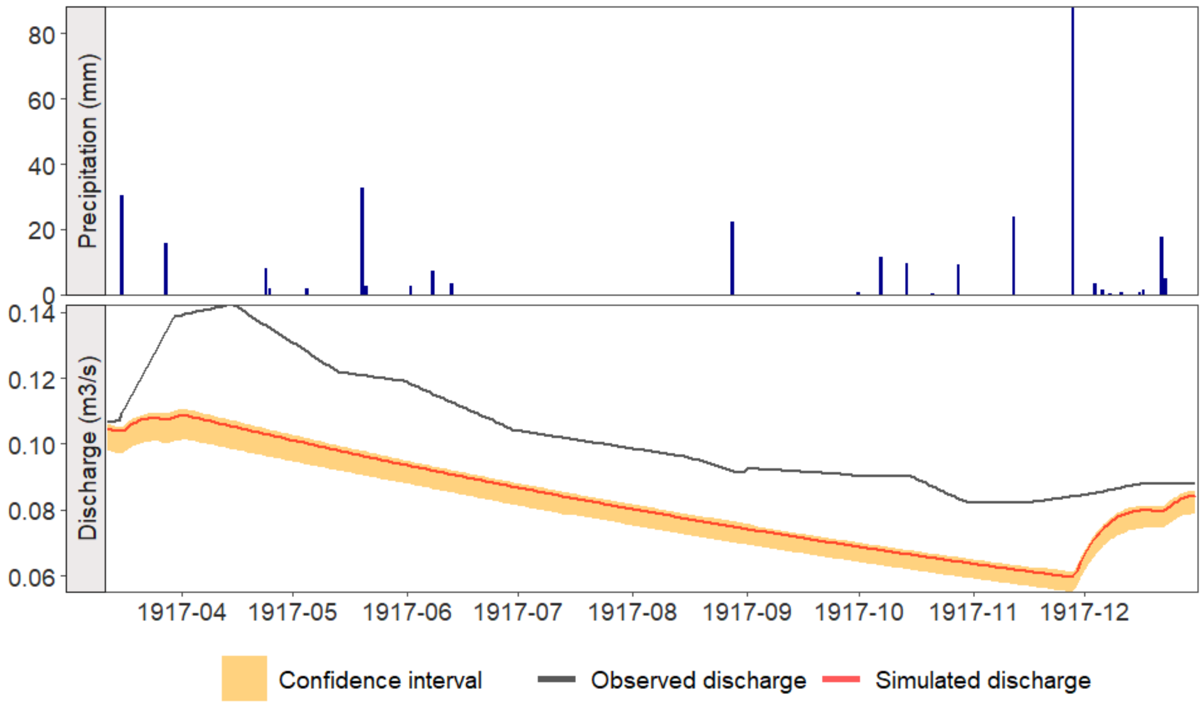

Figure 33: Observed and simulated Zaghouan spring discharge time series (bottom) and precipitation (top) for the validation period.

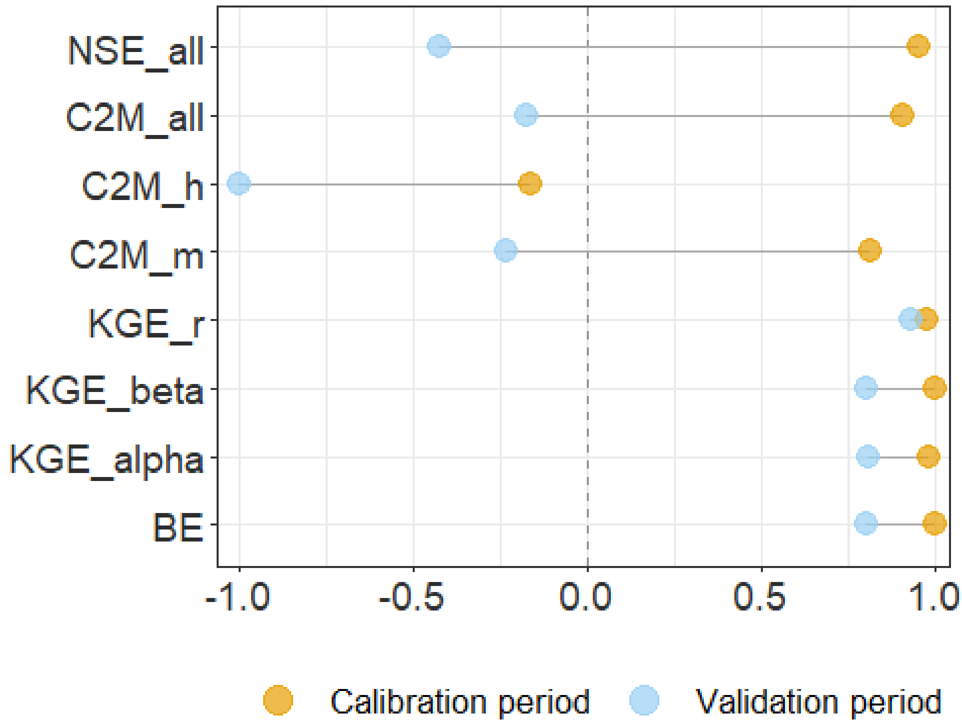

Figure 34: Comparison of the Zaghouan model results through different performance measures on the calibration and validation periods.

On the calibration period, the model simulates very well the observed discharges with a C_{2M} of 0.909 and NSE of 0.953. The inertial dynamics of the system are nicely reproduced, although it seems that the recession coefficient is too extreme. Also, one episode (January 1916) is simulated in the model but was not observed at the spring. As the time series for calibration is very short (1 year), it is difficult to distinguish between uncertainties on discharges and/or precipitation, and lack of model relevance.

On the validation period, the results are really lacking with a C_{2M} of -0.175 and NSE of -0.424. The flood peak is not reproduced on the simulated discharge. It can be due to (i) the non-consideration of the snow accumulation and melt over the catchment, which induces a delayed response at the spring, or (ii) uncertainties on the precipitation time series.

The KGE components indicate a satisfying shape and timing in both calibration (r=0.98) and validation (r=0.93), and very good estimations of discharged volumes (β=1) and flow variability (α=0.98) in calibration. There is a deficit in discharged volumes (β=0.8) and less flow variability (α=0.81) regarding the observed time series in the validation period. It is likely related to a lack in the precipitation input, especially during the flood event in April 1917.

The absence of a fast transfer function in the model structure indicates that the karstification is poor or very poor. The soil available water capacity parameter increases the performance of the model and may translate slow infiltration processes through a poorly transmissive media. Overall, the model seems relevant and could benefit from a longer time series and a refined input data.

7.4 Comparison with APLIS recharge

The Table 5 shows the estimation of the recharge on the KARMA test sites. For each system, we considered an hydrological year with intermediate water conditions (closest to mean annual precipitation) and calculated the recharge with the results of the models. The recharge corresponds to the volume of water that goes into the lower level reservoirs (Q_{EM} and/or Q_{EC}) or directly to the output (Q_{ESO}) during the considered year.

Table 5: Recharge values calculated with the results of the models, in comparison to the results obtained with the APLIS method, and other methods (detailed in Deliverable D2.2).

Country	Spring	Catchment area	Mean annual precipitation	Intermediate hydrological year	Precipitation on intermediate hydrological year	Model Recharge	APLIS Recharge	Other Methods
		km^2	mm		mm	hm^3	hm^3	hm^3
France	Lez	130	904	2010	995	59.8	59.5	87.75
Germany/ Austria	Aubach	9	2089	2014	1873	24.7		44*
Italy	Vacelliera	1.3	1491	2018	1557	1.7		
Lebanon	Qachqouch	56	1258	2017	1027	48.1	25.6	44
Slovenia	Unica	>820	1505	2007	1612	548.4		
Spain	Canamero	NA	900	2008	871	29.8	21.3*	
Spain	Gato Cave	NA	1852	2003	1878	42.4	86.7*	
Tunisia	Zaghouan	19	500	1916	460	1.8		

* The recharge was estimated at the aquifer scale (which may include several springs).

The model recharge estimated on the Lez system (59.8 hm^3) is very close to the recharge estimated with the APLIS method (59.5 hm^3). On Qachqouch system, the model recharge is twice as much (48.1 hm^3) as APLIS recharge (25.6 hm^3). For the two Spanish systems, the APLIS recharge was calculated at the aquifer scale, which can explain the higher value for Gato Cave, but shows a very different estimation for Canamero. The comparison was not possible for the other systems as the APLIS method was not performed at the catchment scale for these systems.

8 Conclusion

We applied the lumped-parameter modelling approach on eight KARMA test sites. The objectives were to study the hydrological functioning of the selected karst systems and identify the main processes at stake. The use of an external snow module allowed to correctly simulate karst spring discharges on five sites that are influenced by snow accumulation and melt. Systemic analyses of precipitation-discharge relationship were applied as preliminary analyses to the modelling approach, in order to better constrain the structure and parameters of the model. The results of the models were contrasted either due to (i) difficulties to reproduce specific hydrological functioning or (ii) uncertainties on the input data. Overall, the simulation results range from very good to satisfying and give relevant insights into the functioning of the systems. The KARMA test sites cover a large variety of hydrological functioning, from very reactive to very inertial, as well as different climate zones. This shows the broad applicability of the developed modeling approach, which is not limited to specific climate or system properties.

We used the classification developed in Task 4.1 to analyze the hydrological functioning of the karst systems. We found that there is an interesting relationship between the determined classes and the structure of the models, which is really valuable as one of the goals of the first task of WP4 was to develop a methodology to help with model conception and parametrization.

The further perspectives of the modelling work are: (i) the development of an internal snow module implemented directly within KarstMod to allow the calibration of the parameters of the routine, and (ii) the comparison of the lumped-parameter modelling approach with ANN modelling approach.

9 References

Algarra, A.M., 1987. Evolucion geologica alpina del contacto entre las zonas internas y las zonas externas de la cordillera Bética (sector centro-occidental) ({http://purl.org/dc/dcmitype/Text}). Universidad de Granada.

Amoruso, A., Crescentini, L., Petitta, M., Tallini, M., 2013. Parsimonious recharge/discharge modeling in carbonate fractured aquifers: The groundwater flow in the Gran Sasso aquifer (Central Italy). Journal of Hydrology 476, 136–146. https://doi.org/10.1016/j.jhydrol.2012.10.026

Andreo, B., Goldscheider, N., Vadillo, I., Vías, J., Neukum, C., Sinreich, M., Gavilán, P., Brechenmacher, J., Carrasco, F., Hötzl, H., Perles, M., Zwahlen, F., 2006. Karst groundwater protection: First application of a Pan-European Approach to vulnerability, hazard and risk mapping in the Sierra de Líbar (Southern Spain). The Science of the total environment 357, 54–73. https://doi.org/10.1016/j.scitotenv.2005.05.019

ARSO, 2021. Ministry of the Environment and Spatial Planning, Slovenian Environment Agency, Archive of hydrological data. Available online: http://vode.arso.gov.si/hidarhiv/.

Avias, J., 1995. Gestion active de l'exsurgence karstique de la source du Lez (Hérault, France) 1957-1994. Hydrogéologie 1, 113–127.

Barberá, J.A., 2014. Investigaciones hidrogeológicas en los acuíferos carbonáticos de la Serranía Oriental de Ronda (Málaga) (PhD thesis). Universidad de Málaga.

Barbieri, M., Boschetti, T., Petitta, M., Tallini, M., 2005. Stable isotope (2H, 18O and 87Sr/86Sr) and hydrochemistry monitoring for groundwater hydrodynamics analysis in a karst aquifer (Gran Sasso, Central Italy). Applied Geochemistry 20, 2063–2081. https://doi.org/10.1016/j.apgeochem.2005.07.008

Bergström, S., 1992. The HBV model - its structure and applications. SMHI 4, 32.

Bergström, S., 1975. THE DEVELOPMENT OF A SNOW ROUTINE FOR THE HBV-2 MODEL. Hydrology Research 6, 73–92. https://doi.org/10.2166/nh.1975.0006

Bicalho, C.C., Batiot-Guilhe, C., Seidel, J.L., Van Exter, S., Jourde, H., 2012. Hydrodynamical changes and their consequences on groundwater hydrochemistry induced by three decades of intense exploitation in a Mediterranean Karst system. Environmental Earth Sciences 65, 2311–2319. https://doi.org/10.1007/s12665-011-1384-2

Chen, Z., Auler, A.S., Bakalowicz, M., Drew, D., Griger, F., Hartmann, J., Jiang, G., Moosdorf, N., Richts, A., Stevanovic, Z., Veni, G., Goldscheider, N., 2017. The World Karst Aquifer Mapping project: Concept, mapping procedure and map of Europe. Hydrogeology Journal 25, 771–785. https://doi.org/10.1007/s10040-016-1519-3

Chen, Z., Goldscheider, N., 2014. Modeling spatially and temporally varied hydraulic behavior of a folded karst system with dominant conduit drainage at catchment scale, HochifenGottesacker, Alps. Journal of Hydrology 514, 41–52.

Chen, Z., Hartmann, A., Wagener, T., Goldscheider, N., 2018. Dynamics of water fluxes and storages in an Alpine karst catchment under current and potential future climate conditions. Hydrology and Earth System Sciences 22, 3807–3823. https://doi.org/10.5194/hess-22-3807-2018

Dausse, A., Leonardi, V., Jourde, H., 2019. Hydraulic characterization and identification of flow-bearing structures based on multi-scale investigations applied to the Lez karst aquifer. Journal of Hydrology: Regional Studies 26, 100627. https://doi.org/10.1016/j.ejrh.2019.100627

Dubois, E., 2017. Analysis of high resolution spring hydrographs and climatic data: Application on the Qachqouch spring (Lebanon) (PhD thesis).

Dubois, E., Doummar, J., Pistre, S., Larocque, M., 2020. Calibration of a semi-distributed lumped karst system model and analysis of its sensitivity to climate conditions: The example of the Qachqouch karst spring (Lebanon) (Preprint). Groundwater hydrology/Modelling approaches. https://doi.org/10.5194/hess-2020-90

Fleury, P., Ladouche, B., Conroux, Y., Jourde, H., Dörfliger, N., 2009. Modelling the hydrologic functions of a karst aquifer under active water management The Lez spring. Journal of Hydrology 365, 235–243. https://doi.org/10.1016/j.jhydrol.2008.11.037

Gabrovšek, F., Kogovšek, J., Kovačič, G., Petrič, M., Ravbar, N., Turk, J., 2010. Recent Results of Tracer Tests in the Catchment of the Unica River (SW Slovenia). Acta Carsologica 39. https://doi.org/10.3986/ac.v39i1.110

Goldscheider, N., 2005. Fold structure and underground drainage pattern in the alpine karst system Hochifen-Gottesacker. Eclogae Geologicae Helvetiae 98, 1–17. https://doi.org/10.1007/s00015-005-1143-z

Gupta, H.V., Kling, H., Yilmaz, K.K., Martinez, G.F., 2009. Decomposition of the mean squared error and NSE performance criteria: Implications for improving hydrological modelling. Journal of Hydrology 377, 80–91. https://doi.org/10.1016/j.jhydrol.2009.08.003

Hartmann, A., Goldscheider, N., Wagener, T., Lange, J., Weiler, M., 2014. Karst water resources in a changing world: Review of hydrological modeling approaches. Reviews of Geophysics 52, 218–242. https://doi.org/10.1002/2013RG000443

Hartmann, A., Lange, J., Aguado, A.V., Mizyed, N., Smiatek, G., Kunstmann, H., 2012. A multi-model approach for improved simulations of future water availability at a large Eastern Mediterranean karst spring. Journal of Hydrology 9.

Hock, R., 1999. A distributed temperature-index ice- and snowmelt model including potential direct solar radiation. Journal of Glaciology 45, 101–111. https://doi.org/10.3189/S0022143000003087

Hogue, T.S., Gupta, H., Sorooshian, S., 2006. A 'User-Friendly' approach to parameter estimation in hydrologic models. Journal of Hydrology 320, 202–217. https://doi.org/10.1016/j.jhydrol.2005.07.009

Jeannin, P.-Y., Artigue, G., Butscher, C., Chang, Y., Charlier, J.-B., Duran, L., Gill, L., Hartmann, A., Johannet, A., Jourde, H., Kavousi, A., Liesch, T., Liu, Y., Lüthi, M., Malard, A., Mazzilli, N., Pardo-Igúzquiza, E., Thiéry, D., Reimann, T., Schuler, P., Wöhling, T., Wunsch, A., 2021. Karst modelling challenge 1: Results of hydrological modelling. Journal of Hydrology 600, 126508. https://doi.org/10.1016/j.jhydrol.2021.126508

Kogovšek, J., Knez, M., Mihevc, A., Petrič, M., Slabe, T., Šebela, S., 1999. Military training area in Kras (Slovenia). Environmental Geology 38, 69–76. https://doi.org/10.1007/s002540050402

Kovačič, G., 2010. Hydrogeological study of the Malenščica karst spring (SW Slovenia) by means of a time series analysis. Acta Carsologica 39. https://doi.org/10.3986/ac.v39i2.93

Kovačič, G., Petrič, M., Ravbar, N., 2020. Evaluation and Quantification of the Effects of Climate and Vegetation Cover Change on Karst Water Sources: Case Studies of Two Springs in South-Western Slovenia. Water 12, 3087. https://doi.org/10.3390/w12113087

Lehmann, P., Stauffer, F., Hinz, C., Dury, O., Flühler, H., 1998. Effect of hysteresis on water flow in a sand column with a fluctuating capillary fringe. Journal of Contaminant Hydrology 33, 81–100. https://doi.org/10.1016/S0169-7722(98)00066-7

Mangin, A., 1971. Etude des débits classés d'exutoires karstiques portant sur un cycle hydrologique. Annales de spéléologie 26, 283–329.

Mathevet, T., Michel, C., Andréassian, V., Perrin, C., 2009. A bounded version of the Nash-Sutcliffe criterion for better model assessment on large sets of basins 9.

Mayaud, C., Gabrovšek, F., Blatnik, M., Kogovšek, B., Petrič, M., Ravbar, N., 2019. Understanding flooding in poljes: A modelling perspective. Journal of Hydrology 575, 874–889. https://doi.org/10.1016/j.jhydrol.2019.04.092

Mazzilli, N., 2011. Sensibilité et incertitude de modélisation sur les bassins à forte composante karstique (PhD thesis). Université de Montpellier.

Mazzilli, N., Bertin, D., 2019. KarstMod User Guide - version 2.2 hal-01832693, 103927.

Mazzilli, N., Guinot, V., Jourde, H., Lecoq, N., Labat, D., Arfib, B., Baudement, C., Danquigny, C., Dal Soglio, L., Bertin, D., 2017. KarstMod: A modelling platform for rainfall - discharge analysis and modelling dedicated to karst systems. Environmental Modelling & Software 122, 103927. https://doi.org/10.1016/j.envsoft.2017.03.015

Nash, J.E., Sutcliffe, J., 1970. River flow forecasting through conceptual models : Part 1. A discussion of principles. Journal of Hydrology 10, 282–290.

Padilla, A., Pulido-Bosch, A., 1995. Study of hydrographs of karstic aquifers by means of correlation and cross-spectral analysis. Journal of Hydrology 168, 73–89. https://doi.org/10.1016/0022-1694(94)02648-U

Peel, M.C., Finlayson, B.L., McMahon, T.A., 2007. Updated world map of the Koppen-Geiger climate classification. Hydrology and Earth System Sciences 11, 1633–1644. https://doi.org/10.5194/hess-11-1633-2007

Perrin, C., Michel, C., Andréassian, V., 2001. Does a large number of parameters enhance model performance? Comparative assessment of common catchment model structures on 429 catchments. Journal of Hydrology 242, 275–301. https://doi.org/10.1016/S0022-1694(00)00393-0

Petaccia, R., Rusi, S., 2008. Idrogeologia delle sorgenti del Ruzzo (Gran Sasso d'Italia). Giornale di Geologia Applicata 8, 17–28. https://doi.org/10.1474/GGA.2008-08.1-02.0212

Petric, M., 2010. Chapter 10.3 - Case Study: Characterization, exploitation, and protection of the Malenščica karst spring, Slovenia, in: Kresic, N., Stevanovic, Z. (Eds.), Groundwater Hydrology of Springs. Butterworth-Heinemann, Boston, pp. 428–441. https://doi.org/10.1016/B978-1-85617-502-9.00021-9

Ravbar, N., Mayaud, C., Blatnik, M., Petrič, M., 2021. Determination of inundation areas within karst poljes and intermittent lakes for the purposes of ephemeral flood mapping. Hydrogeology Journal 29, 213–228. https://doi.org/10.1007/s10040-020-02268-x

Refsgaard, J.C., van der Sluijs, J.P., Højberg, A.L., Vanrolleghem, P.A., 2007. Uncertainty in the environmental modelling process A framework and guidance. Environmental Modelling & Software 22, 1543–1556. https://doi.org/10.1016/j.envsoft.2007.02.004

Santos, L., Thirel, G., Perrin, C., 2018. Technical note: Pitfalls in using log-transformed flows within the KGE criterion. Hydrology and Earth System Sciences 22, 4583–4591. https://doi.org/10.5194/hess-22-4583-2018

Stevanović, Z., 2019. Karst waters in potable water supply: A global scale overview. Environmental Earth Sciences 78, 662. https://doi.org/10.1007/s12665-019-8670-9

Thiéry, D., Bérard, P., 1983. Alimentation en eau de la ville de Montpellier - captage de la source du Lez - études des relations entre la source et son réservoir aquifère. ({{BRGM}} No. 83).

Tritz, S., Guinot, V., Jourde, H., 2011. Modelling the behaviour of a karst system catchment using non-linear hysteretic conceptual model. Journal of Hydrology 397, 250–262. https://doi.org/10.1016/j.jhydrol.2010.12.001

10 Appendix

Lez - Class C2

Display of the selected recession curves

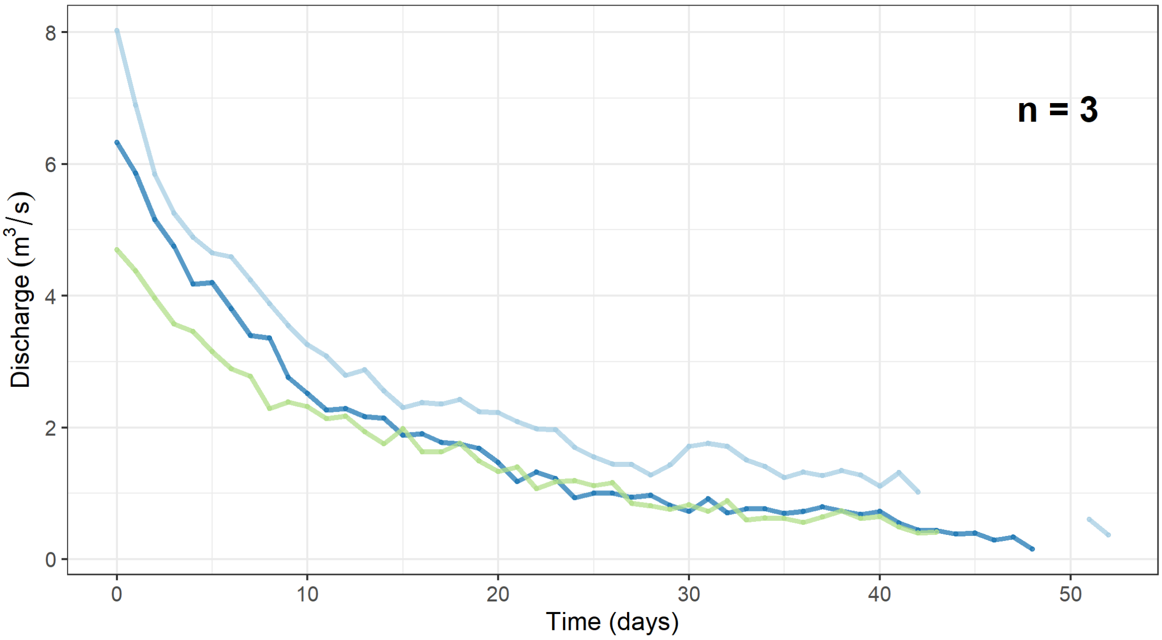

Indicators details

N°	k	i	alpha
1	0.09	0.62	0.03
2	0.04	0.71	0.047
3	0.02	0.61	0.047

Curve of classified discharges

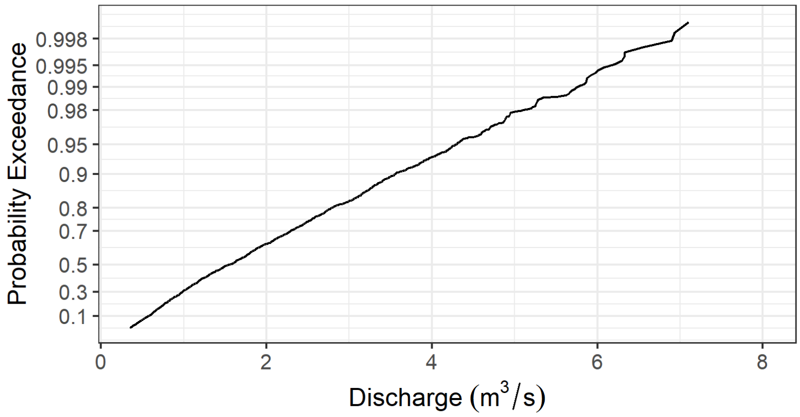

Characterization of the hydrological functioning

kmax = 0.09 -> Very low to Low capacity of dynamic storage

alpha = 0.042 -> Very high draining dynamic of the capacitive function

IR = 0.1 -> Medium variability of the hydrological response

RT = NA -> No value to interpret

Appendix 1: Lez classification

Aubach - Class C2

Display of the selected recession curves

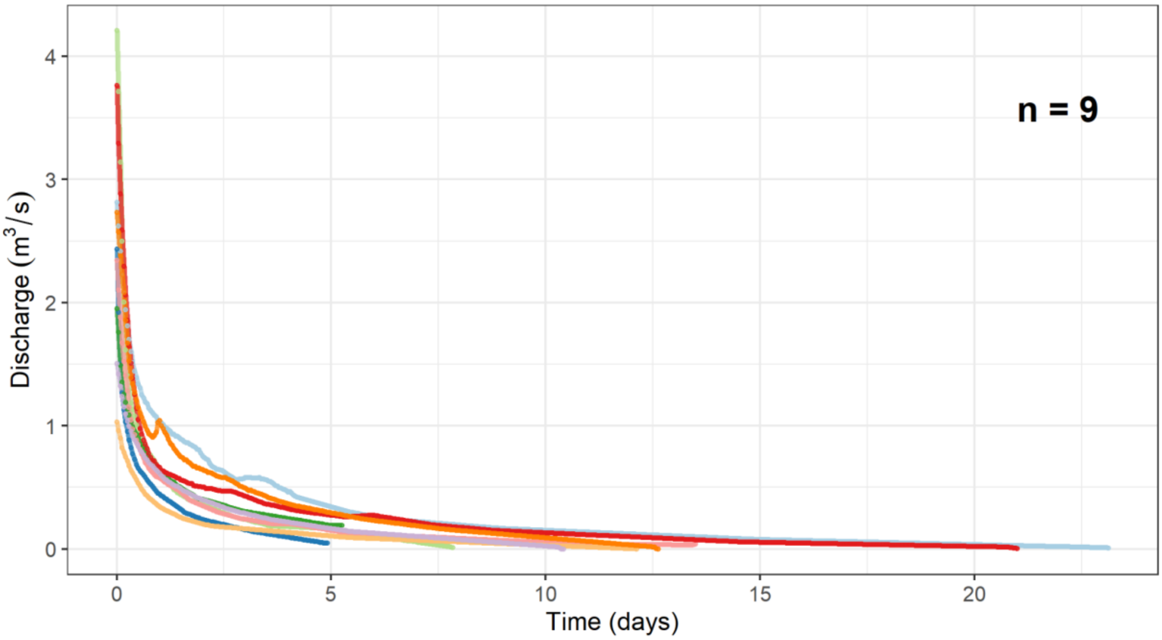

Indicators details

N°	k	i	alpha
1	0	0.11	0.136
2	0	0	0.497
3	0	0.01	0.309
4	0	0.01	0.238
5	0	0.03	0.215
6	0.01	0.03	0.158
7	0	0.02	0.232
8	0.01	0.01	0.254
9	0	0.03	0.283

Curve of classified discharges

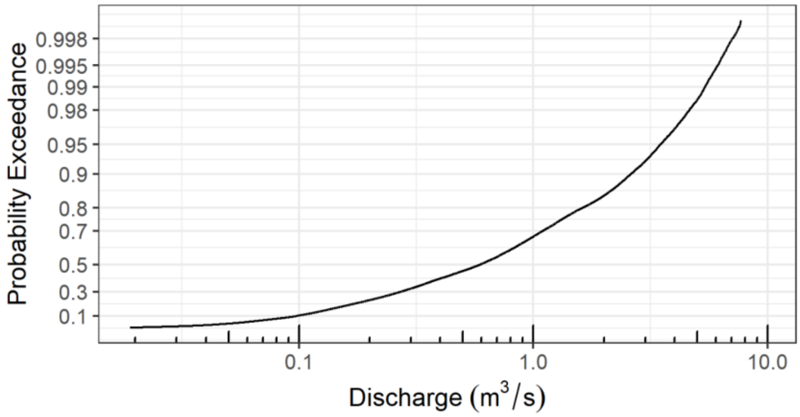

Characterization of the hydrological functioning

kmax = 0.01 -> Very low to Low capacity of dynamic storage

alpha = 0.258 -> Very high draining dynamic of the capacitive function

IR = 0.11 -> Medium variability of the hydrological response

RT = 25.9 -> Medium global inertia

Appendix 2: Aubach classification

Vacelliera - Class C6

Display of the selected recession curves

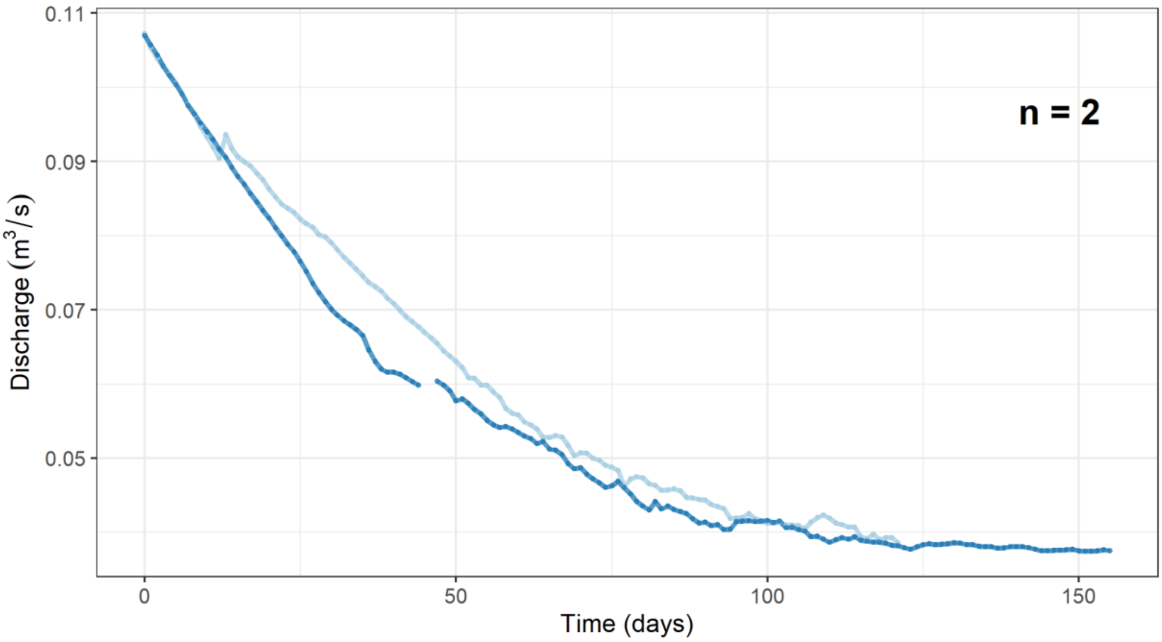

Indicators details

N°	k	i	alpha
1	0.43	0.96	0.005
2	1.99	0.95	0.001

Curve of classified discharges

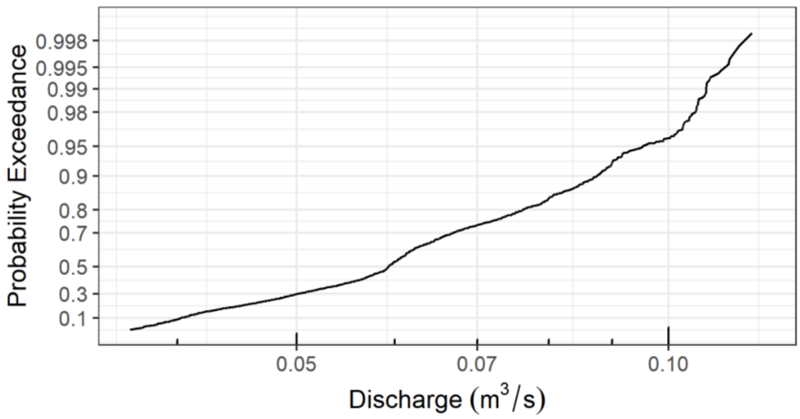

Characterization of the hydrological functioning

kmax = 1.99 -> High to Very high capacity of dynamic storage

alpha = 0.003 -> Low draining dynamic of the capacitive function

IR = 0.01 -> Low variability of the hydrological response

RT = 52.2 -> Very high global inertia

Appendix 3: Vacelliera classification

Qachqouch - Class C3

Display of the selected recession curves

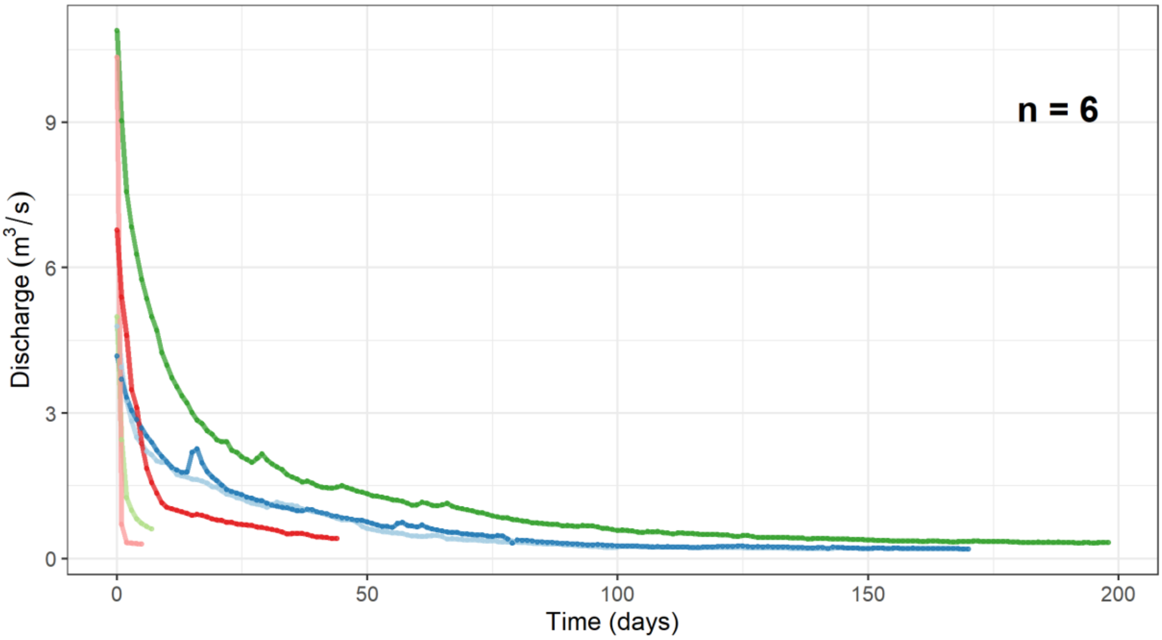

Indicators details

N°	k	i	alpha
1	0.06	0.74	0.007
2	0.1	0.84	0.003
3	0.01	0.14	0.099
4	0.11	0.7	0.006
5	0.01	0.01	0.029
6	0.05	0.57	0.028

Curve of classified discharges

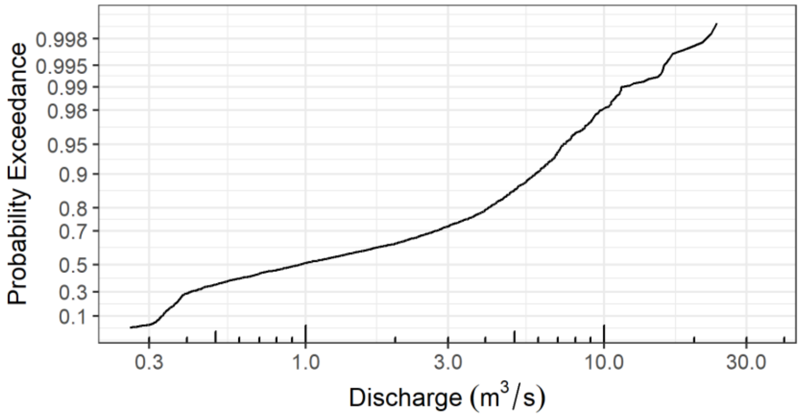

Characterization of the hydrological functioning

kmax = 0.11 -> Very low to Low capacity of dynamic storage

alpha = 0.029 -> Fast draining dynamic of the capacitive function

IR = 0.83 -> Very high variability of the hydrological response

RT = 30.09 -> High global inertia

Appendix 4: Qachqouch classification

Unica - Class C3

Display of the selected recession curves

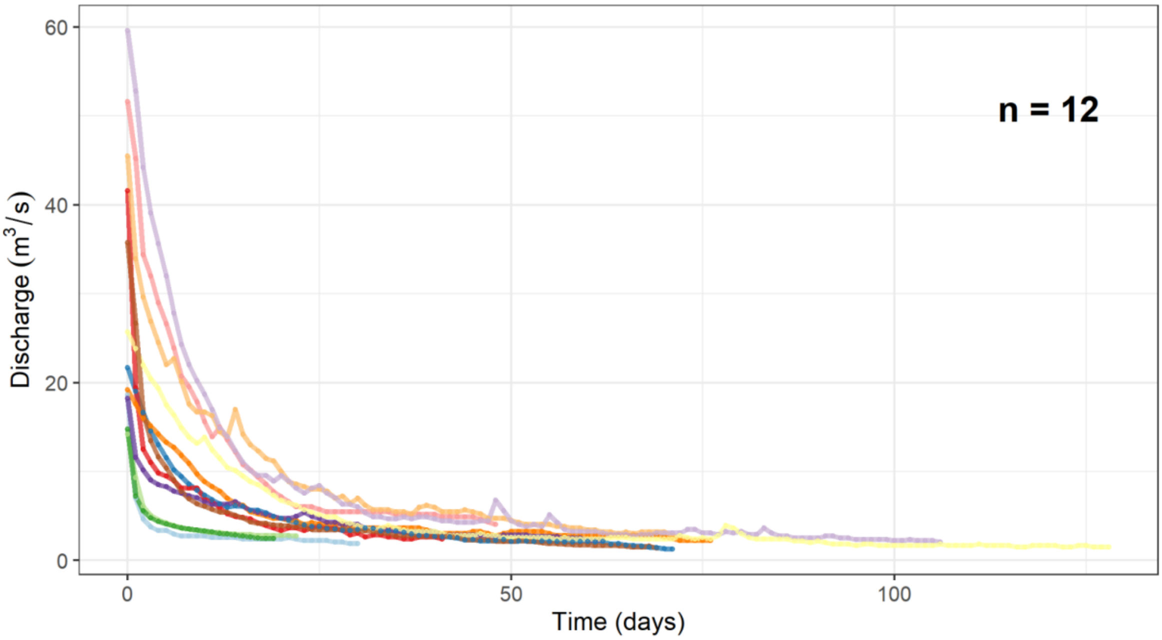

Indicators details

N°	k	i	alpha
1	0.02	0.11	0.015
2	0.07	0.68	0.01
3	0.02	0.24	0.023
4	0.04	0.61	0.019
5	0.05	0.77	0.01
6	0.05	0.69	0.012
7	0.03	0.46	0.013
8	0.05	0.81	0.008
9	0.02	0.39	0.02
10	0.02	0.63	0.019
11	0.02	0.27	0.018
12	0.01	0.13	0.035

Curve of classified discharges

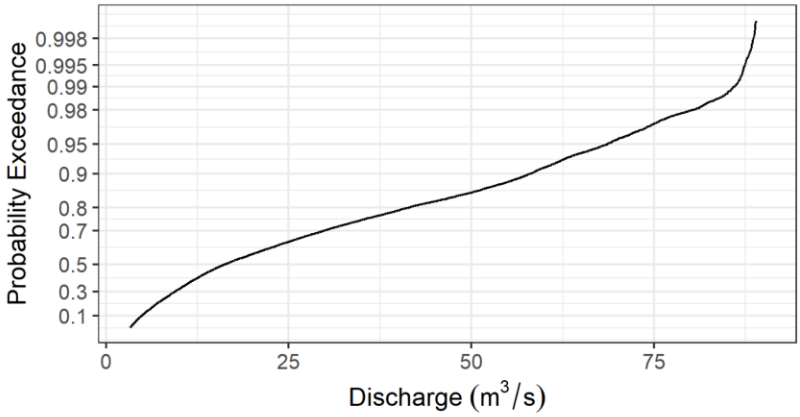

Characterization of the hydrological functioning

kmax = 0.07 -> Very low to Low capacity of dynamic storage

alpha = 0.017 -> High draining dynamic of the capacitive function

IR = 0.7 -> Very high variability of the hydrological response

RT = 38.9 -> High global inertia

Appendix 5: Unica classification

Canamero - Class C4

Display of the selected recession curves

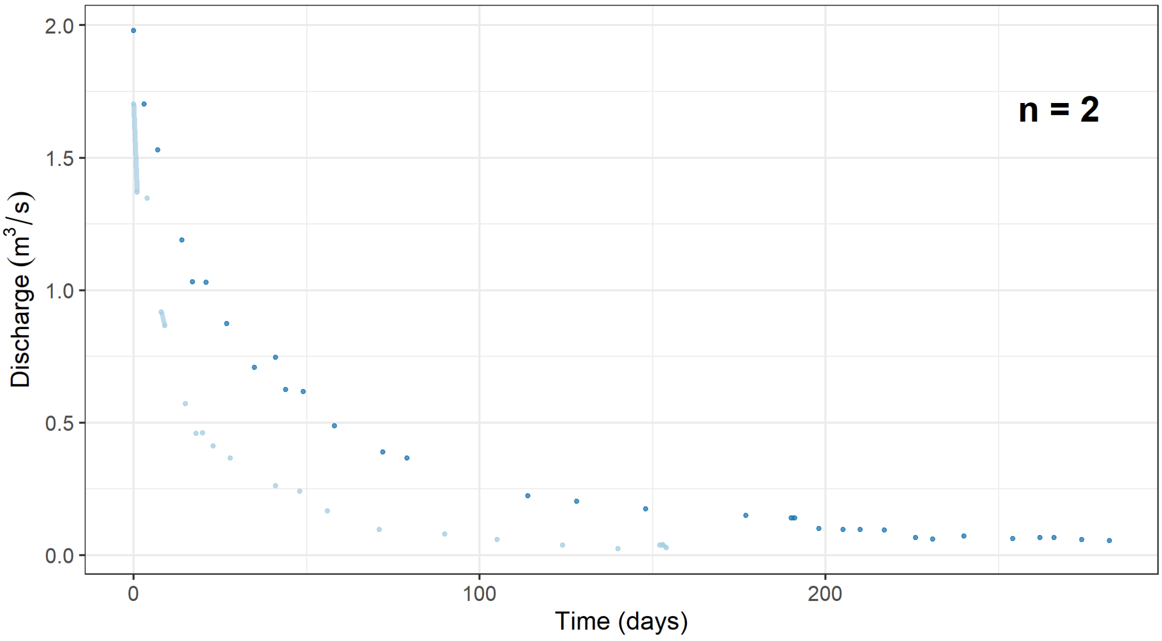

Indicators details

N°	k	i	alpha
1	0.02	0.75	0.019
2	0.05	0.87	0.009

Curve of classified discharges

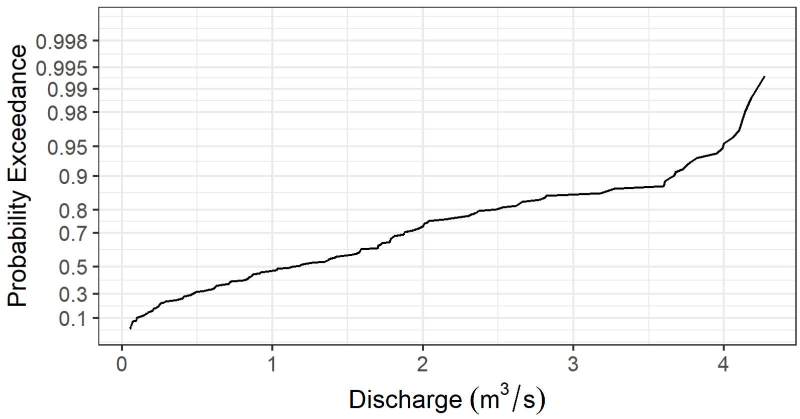

Characterization of the hydrological functioning

kmax = 0.05 -> Very low to Low capacity of dynamic storage

alpha = 0.014 -> Medium draining dynamic of the capacitive function

IR = 0.11 -> Medium variability of the hydrological response

RT = NA -> No value to interpret

Appendix 6: Canamero classification

Gato Cave - Class C4

Display of the selected recession curves

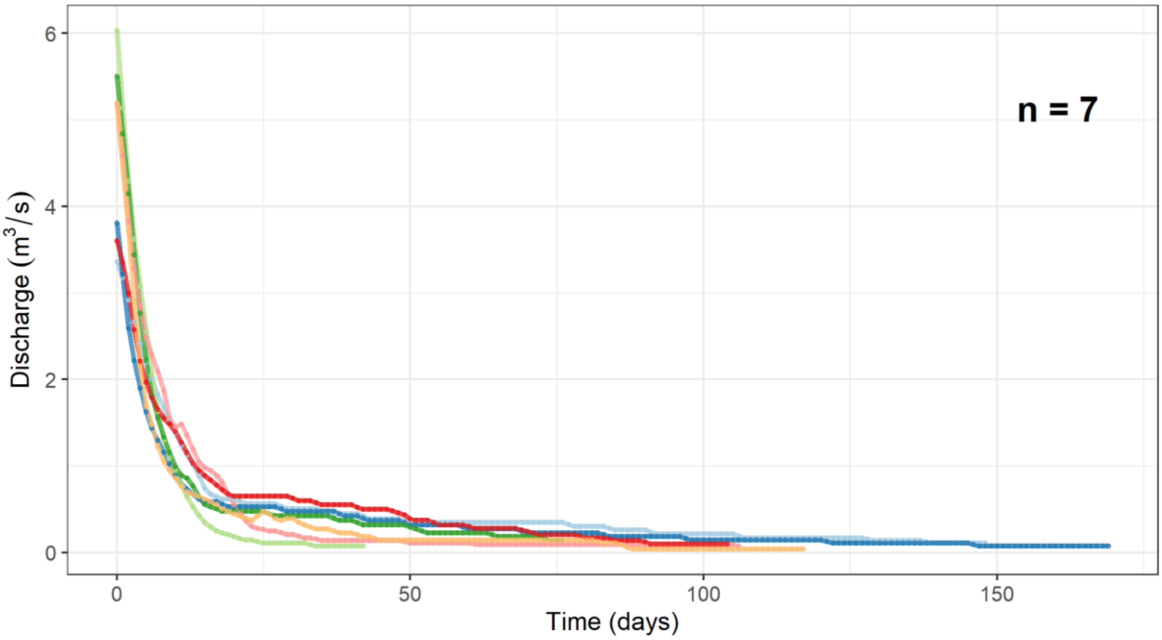

Indicators details

N°	k	i	alpha
1	0.09	0.81	0.013
2	0.07	0.61	0.015
3	0.01	0.65	0.066
4	0.05	0.64	0.02
5	0.03	0.72	0.013
6	0.06	0.69	0.022
7	0.03	0.56	0.026

Curve of classified discharges

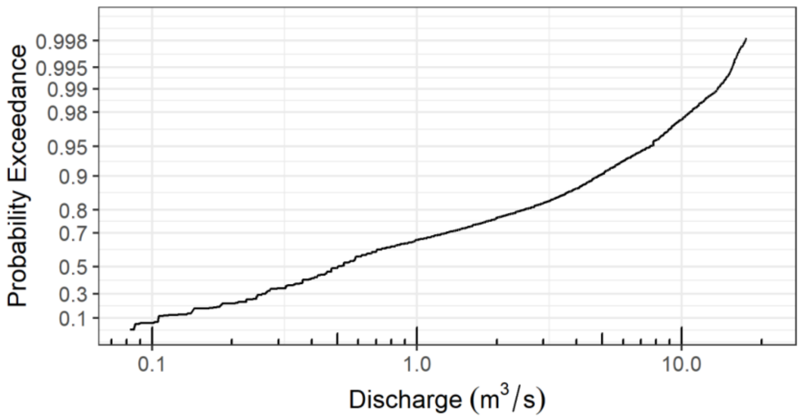

Characterization of the hydrological functioning

kmax = 0.09 -> Very low to Low capacity of dynamic storage

alpha = 0.025 -> High draining dynamic of the capacitive function

IR = 0.25 -> Medium variability of the hydrological response

RT = 43.65 -> High global inertia

Appendix 7: Gato Cave classification

Zaghouan - Class C6

Display of the selected recession curves

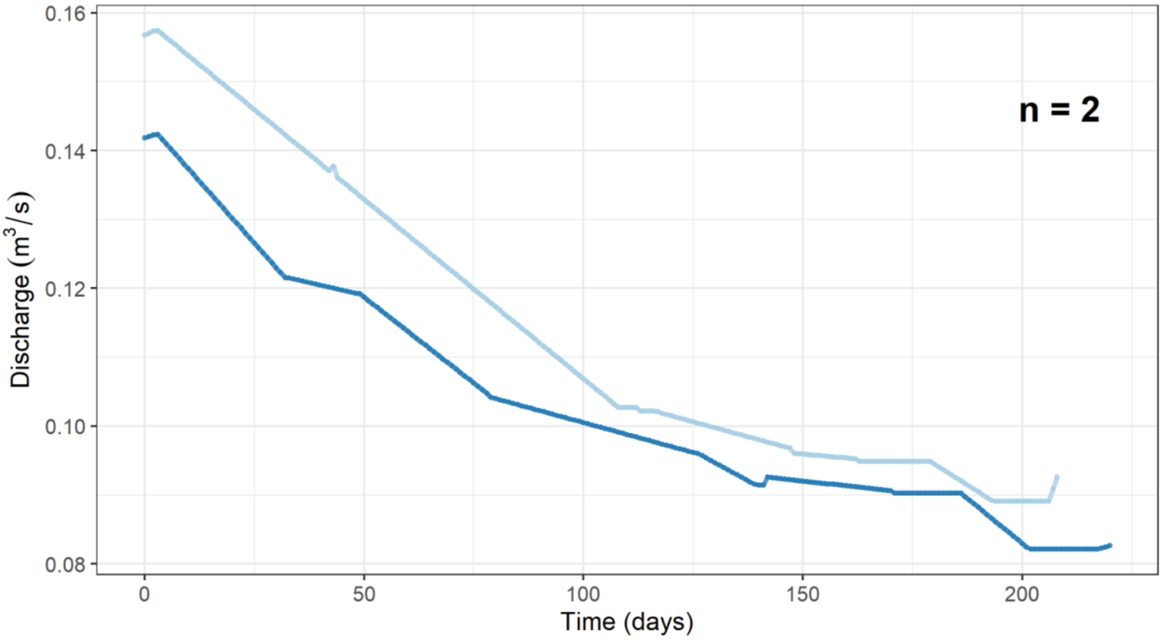

Indicators details

N°	k	i	alpha
1	1.91	0.98	0.001
2	1.6	0.95	0.002

Curve of classified discharges

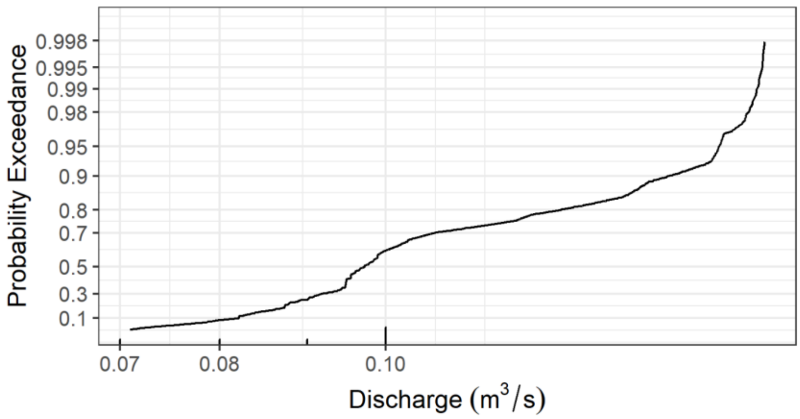

Characterization of the hydrological functioning

kmax = 1.91 -> High to Very high capacity of dynamic storage

alpha = 0.002 -> Low draining dynamic of the capacitive function

IR = 0.03 -> Low variability of the hydrological response

RT = 76.88 -> Very high global inertia

Appendix 8: Zaghouan classification